Loss of primary cilia promotes inflammation and carcinogenesis

Conception Paul, Ruizhi Tang, Ciro Longobardi, Rossano Lattanzio, Thibaut Eguether, Hulya Turali, Julie Bremond, Chloé Maurizy, Monica Gabola, Sophie Poupeau, et al.

Article

TRANSPARENT PROCESS OPEN ACCESS

EMBO reports

Loss of primary cilia promotes inflammation and carcinogenesis

Conception Paul[1,†], Ruizhi Tang[1,†], Ciro Longobardi[1,2,3], Rossano Lattanzio[4], Thibaut Eguether[5], Hulya Turali[1], Julie Bremond[1], Chloé Maurizy[1], Monica Gabola[1], Sophie Poupeau[1], Andrei Turtoi[6], Emilie Denicolai[7], Maria Concetta Cufaro[4], Magali Svrcek[8], Philippe Seksik[5], Vincent Castronovo[9], Philippe Delvenne[7,10], Vincenzo de Laurenzi[4], Quentin Da Costa[7], François Bertucci[7], Bénédicte Lemmers[1], Damiana Pieragostino[4], Emilie Mamessier[7], Carsten Janke[11,12], Valérie Pinet[1,*,‡] & Michael Hahne[1,**,‡]

Abstract

Primary cilia (PC) are important signaling hubs, and we here explored their role in colonic pathology. In the colon, PC are mostly present on fibroblasts, and exposure of mice to either chemically induced colitis-associated colon carcinogenesis (CAC) or dextran sodium sulfate (DSS)-induced acute colitis decreases PC numbers. We generated conditional knockout mice with reduced numbers of PC on colonic fibroblasts. These mice show increased susceptibility to CAC, as well as DSS-induced colitis. Secretome and immunohistochemical analyses of DSS-treated mice display an elevated production of the proinflammatory cytokine IL-6 in PC-deficient colons. An inflammatory environment diminishes PC presence in primary fibroblast cultures, which is triggered by IL-6 as identified by RNA-seq analysis together with blocking experiments. These findings suggest an activation loop between IL-6 production and PC loss. An analysis of PC presence on biopsies of patients with ulcerative colitis or colorectal cancer (CRC) reveals decreased numbers of PC on colonic fibroblasts in pathological compared with surrounding normal tissue. Taken together, we provide evidence that a decrease in colonic PC numbers promotes colitis and CRC.

Keywords colitis; colon carcinogenesis; colonic fibroblasts; primary cilia; inflammation

Subject Categories Cancer; Cell Adhesion, Polarity & Cytoskeleton; Immunology

DOI 10.15252/embr.202255687 | Received 30 June 2022 | Revised 9 September 2022 | Accepted 4 October 2022

EMBO Reports (2022) e55687

Introduction

Colorectal cancer (CRC) remains the third most common cause of cancer death in the western world (Malvezzi *et al*, 2018). CRC is a highly heterogenous disease and frequently diagnosed only after cancer has spread through the colon or rectal wall (stage II), to the lymph nodes (stage III) and/or to distant organs (stage IV), for example, liver, lung, and peritoneum. Most patients receiving standard-of-care treatment relapse within 5 years, highlighting the need to develop novel biomarker-guided therapeutic approaches to improve the treatment of CRC patients. A meta-analysis identified the existence of 4 distinct gene expression–based Consensus Molecular Subtypes (CMS) of CRC carcinoma, that is, immune (CMS1),

1 Institut de Génétique Moléculaire de Montpellier, Univ Montpellier, CNRS, Label "Equipe FRM", Montpellier, France
2 Center for Experimental and Molecular Medicine, Cancer Center Amsterdam, Amsterdam UMC, University of Amsterdam, Amsterdam, The Netherlands
3 Oncode Institute, Amsterdam UMC, University of Amsterdam, Amsterdam, The Netherlands
4 Department of Innovative Technologies in Medicine & Dentistry, Center for Advanced Studies and Technology (CAST), 'G. d'Annunzio' University of Chieti–Pescara, Chieti, Italy
5 Centre de Recherche Saint Antoine, Sorbonne Université, INSERM, APHP, Paris, France
6 Tumor Microenvironment and Resistance to Treatment Laboratory, Institut de Recherche en Cancérologie de Montpellier, Montpellier, France
7 Cancer Research Center of Marseille (CRCM), Laboratory of Predictive Oncology, Inserm U1068 - CNRS UMR7258 – University of Aix-Marseille UM105 - Paoli Calmettes Institute (IPC), Label "Ligue contre le cancer", Marseille, France
8 Department of Pathology, AP-HP, Hôpital Saint-Antoine, Sorbonne Université, Paris, France
9 Metastasis Research Laboratory, GIGA Cancer, University of Liège, Liège, Belgium
10 Department of Pathology, University Hospital (CHU), University of Liège, Liège, Belgium
11 Institut Curie, Paris Sciences et Lettres (PSL) Research University, Centre National de la Recherche Scientifique (CNRS) Unité Mixte de Recherche (UMR) 3348, Label "Equipe FRM", Orsay, France
12 Université Paris Sud, Université Paris-Saclay, CNRS UMR 3348, Orsay, France
*Corresponding author. Tel: +33 4 34 35 96 38; E-mail: michael.hahne@igmm.cnrs.fr
**Corresponding author. Tel: +33 4 34 35 96 38; E-mail: valerie.pinet@igmm.cnrs.fr
†These authors contributed equally to this work as first authors
‡These authors contributed equally to this work as senior authors

canonical (CMS2), metabolic (CMS3), and mesenchymal (CMS4) subtypes, among which only CMS2 patients respond well to standard-of-care therapy (Guinney *et al*, 2015). CMS4 cancers, in which inflammation and fibroblasts are key drivers, have the worst survival rate. Notably, premalignant adenomas can also be stratified according to the CMS subtypes (Fessler *et al*, 2016).

Interventions, which can be made at the early stages of tumor development, would increase the treatment efficiency. This is hampered at present, as the biology of pretumoral lesions in CRC is still poorly understood. It is estimated that only 5% of colonic adenoma progress to carcinoma. Thus, reliable indicators still need to be established, which would allow identifying lesions with high malignant potential. This includes a better understanding of the crosstalk between premalignant cells and cells of the microenvironment, among which are colonic fibroblasts (CF).

An underexplored trait in the cellular crosstalk is primary cilia (PC), an antennae-like structure extruding from the surface of many mammalian cells. PC are cellular organelles serving as sensors of environmental signals (Gerdes *et al*, 2009). They contain a scaffold of nine microtubule (MT) doublets forming a cylinder-like arrangement in the plasma membrane by a basal body that derives from a centriole. Abnormal ciliary function result in so-called ciliopathies, that is, inherited disorders, such as cystic kidney diseases (Ko & Park, 2013). *In vitro* studies suggest an inflammation counteracting role of PC (Choi *et al*, 2021) and indeed, certain ciliopathies display inflammation (Song *et al*, 2017).

PC can be also involved in tumor formation and a concept is emerging that there is an important inter- and intra-tumoral variation of PC presence (Eguether & Hahne, 2018; Liu *et al*, 2018). PC properties can be modulated by post-translational modifications (PTMs) of tubulin including acetylation and glycylation (Wloga *et al*, 2017). For example, it has been shown that blocking of deacetylation induces cilia restoration and decreases tumor growth of cholangiocarcinoma (Gradilone *et al*, 2013). We previously described an unexpected role of the tubulin glycylase TTLL3 in the regulation of colon tumorigenesis (Rocha *et al*, 2014). Specifically, we discovered that TTLL3 is the only glycylase expressed in the colon and that the absence of TTLL3 leads to decreased numbers of colonic PC (Rocha *et al*, 2014). When exposed to chemically induced colitis-associated colon carcinogenesis, *Ttll3*$^{-/-}$ mice are more susceptible to tumor formation (Rocha *et al*, 2014). Importantly, TTLL3 expression levels were significantly downregulated in human primary colorectal carcinomas and metastases as compared to healthy colon tissue, strongly suggesting a pivotal role of TTLL3 in colorectal cancer. Altogether, these findings reveal a correlation between TTLL3, loss of PC, and colon carcinogenesis. However, it cannot be excluded that TTLL3-catalyzed glycylation has nonciliary functions, especially because other substrates than tubulin can be glycylated. For instance, we observed glycylation of additional proteins in glycylase overexpressing cells (fig 1D in Gadadhar *et al*, 2017). The role of glycylation of these proteins is not yet explored and a contribution during colon carcinogenesis can therefore not be excluded.

In this study, we set out to corroborate the involvement of PC in colonic pathologies by employing relevant mouse models and analyzing patients' biopsies.

Results

Colonic fibroblasts form primary cilia

To characterize the presence of PC in the colon we employed a previously described protocol that allows the detection of PC on paraffin-embedded tissues (Coy *et al*, 2016). Indeed, this protocol allows to overcome the technical limitations we previously faced in detecting PC on cryosections of the colon and identifying which colonic cell subsets display PC (Rocha *et al*, 2014). Co-staining was performed by combining the established PC marker Arl13b (Caspary *et al*, 2007) with markers for epithelial or stromal cells including E-cadherin, vimentin, alpha-smooth muscle actin (α-SMA) and CD140a (platelet-derived growth factor receptor alpha; Fig 1A–D). Vimentin is a pan-fibroblast marker, α-SMA identifies myofibroblasts, whereas CD140a characterizes a subpopulation of fibroblasts present on the upper parts of the crypts (Kurahashi *et al*, 2013; Roulis & Flavell, 2016; Fig 1B–D). While only few epithelial cells displayed detectable PC (Figs 1A and EV1), PC were mostly found on vimentin^{positive} or CD140a^{positive} stromal cells in the lamina propria (Fig 1B–D) but also on α-SMA^{positive} myofibroblasts (Fig 1D).

Progressive loss of colonic primary cilia during colon carcinogenesis

To determine how PC presence relates to colon carcinogenesis, we quantified the number of PC in a mouse model that mimics colitis-associated colon carcinogenesis (CAC) (Suzuki *et al*, 2004; Tanaka, 2012). This model depends on the administration of the mutagen azoxymethane (AOM) and the subsequent induction of inflammation with dextran sodium sulfate (DSS) (Fig 2A). DSS is toxic to mucosal epithelial cells in the colon, and the ensuing breakdown of the mucosal barrier leads to inflammation. The CAC mouse model allows to follow the progression from preneoplastic lesions to adenocarcinoma within 60 days. In this model, PC on vimentin^{positive} cells in tumor lesions was lower as compared to adjacent normal mucosa (Fig 2B and C). Remarkably, colon areas with high-grade dysplasia showed significantly lower numbers of PC than those with low-grade dysplasia. Taken together, CAC is associated with the downregulation of PC, confirming our initial hypothesis.

Decreased numbers of primary cilia in colonic fibroblasts promote CAC

To establish a causal relationship of PC on colonic fibroblasts and the development of CRC, we employed a mouse strain carrying

Figure 1. Primary cilia in the colon are mostly present on stromal cells.

A–D PC were identified by immunostaining for Arl13b (in green except in (D); arrowheads in the panel on the right-hand side), and in parallel by identifying epithelial cells with E-cadherin (A), fibroblasts with vimentin (B), and CD140a (C), labeling (all in red), and myofibroblasts by α-SMA stain (D) (in green). Nuclei were stained with DAPI (in blue). Scale bars represent 30, 10, and 3 μm, respectively (from the left to the right).

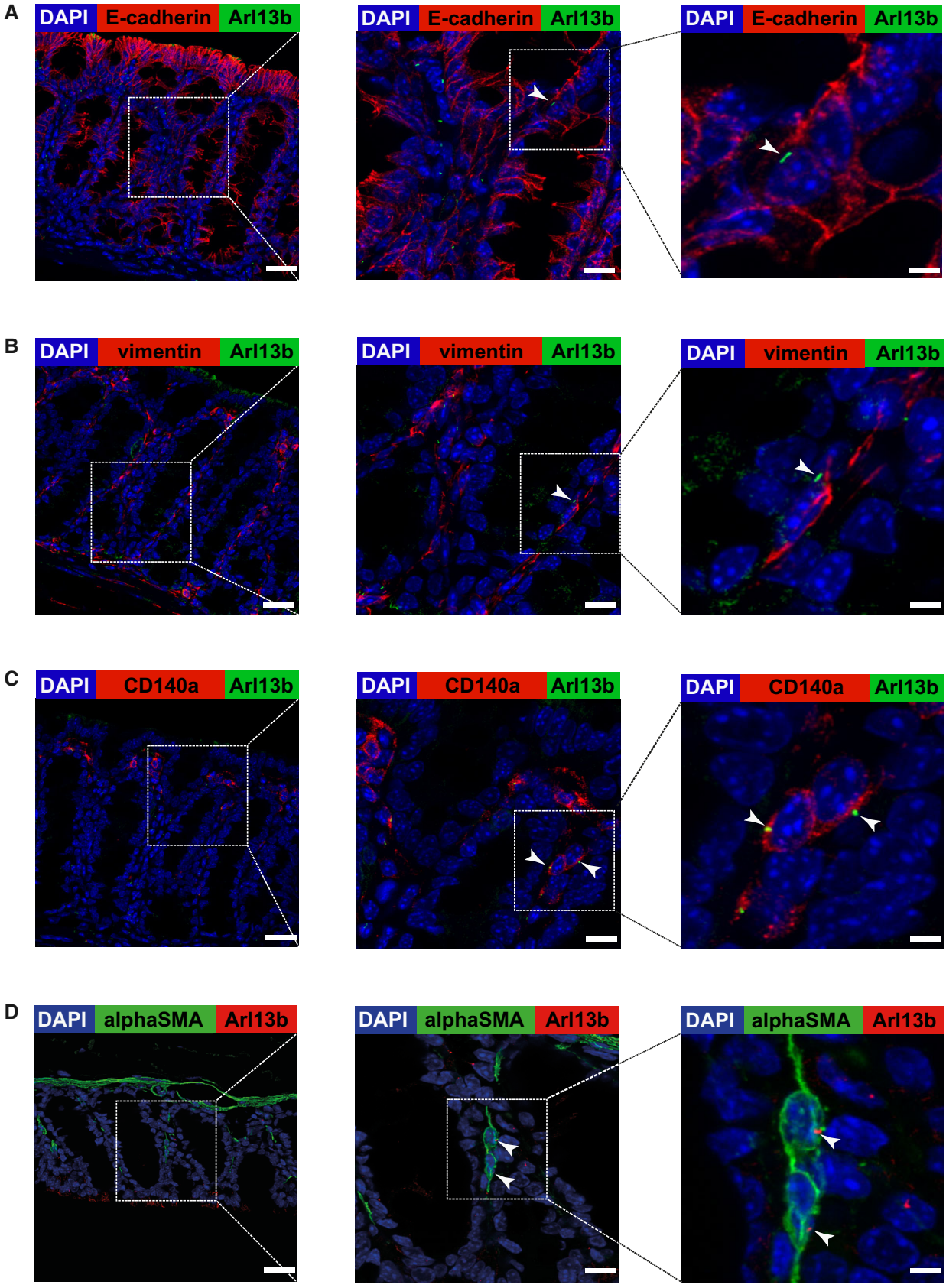

Figure 1.

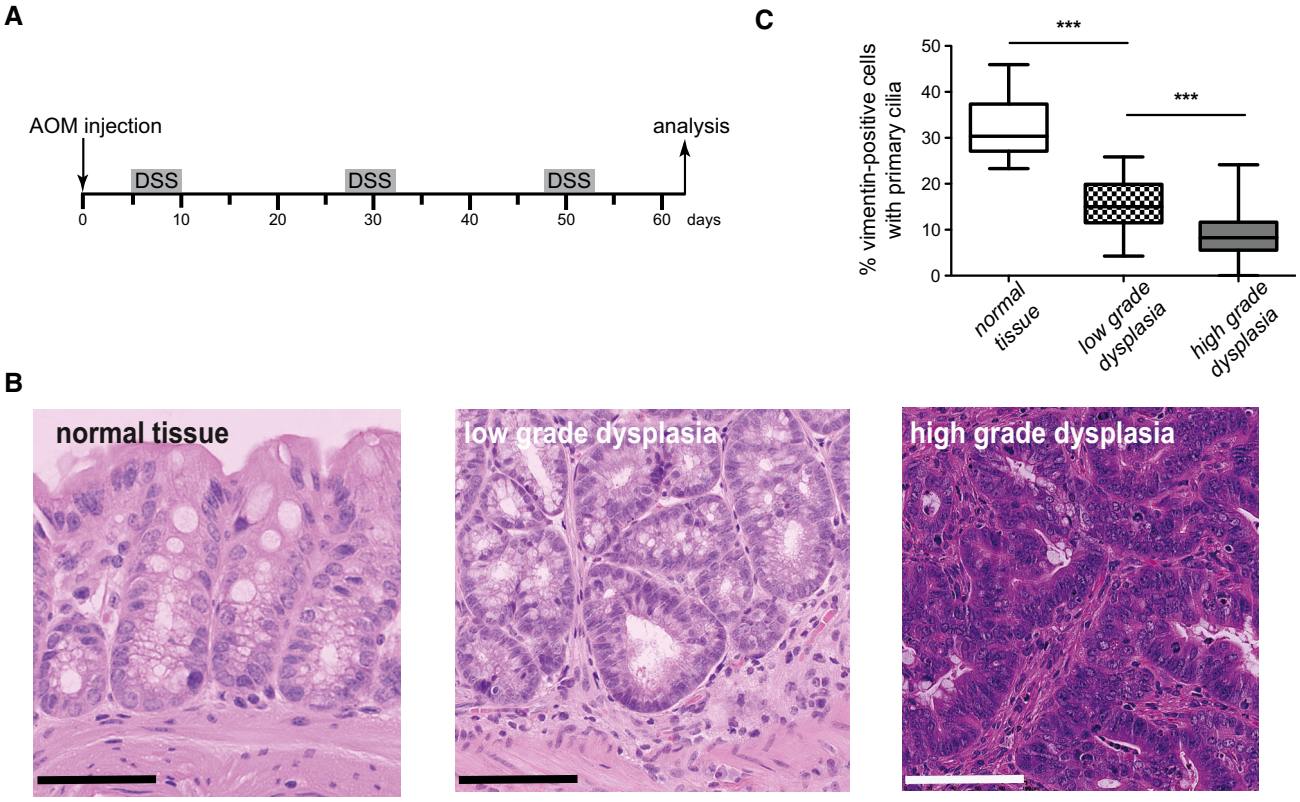

Figure 2. The number of colonic primary cilia decreases during colon carcinogenesis.

A Experimental timeline for azoxymethane (AOM)/dextran sodium sulfate (DSS)-induced CAC.

B Hematoxylin/Eosin staining of paraffin-sections from normal colon and colon of AOM/DSS-treated C57Bl/6 mice as indicated in (A). Representative areas of normal colon and colon with low- and high-grade dysplasia are shown. Features include hyperchromasia, stratification, and elongated cell nuclei in low-grade dysplasia and marked hyperchromasia and increased pleomorphism of nuclei, as well as loss of cell polarity in high-grade dysplasia. Scale bars represent 100 μm.

C Box-and-whisker plots showing quantitative analysis of PC expression on vimentin$^+$ cells in normal colon, and colon with low- and high-grade dysplasia in mice exposed to the AOM/DSS protocol (analyzing at least 12 fields depicted from four different mice as illustrated in the middle and right panel of (B)). The box plot shows the median (inside line), 25–75 percentiles (box bottom to top), and the Whiskers connect the minimum and the maximum values to the Box. Significance values were determined by two-tailed unpaired *t*-tests (***$p < 10^{-3}$).

conditional knockout (KO) alleles for the kinesin family member 3A (*Kif3a*$^{flx/flx}$; Marszalek *et al*, 1999), a protein essential for cilia formation. Deletion of this gene in intestinal fibroblasts was achieved through crossing with *ColVIcre* transgenic mice, expressing Cre DNA-recombinase under the control of a collagenase VI promoter (Armaka *et al*, 2008; Koliaraki *et al*, 2015; Roulis & Flavell, 2016). *ColVIcre-Kif3a*$^{flx/flx}$ mice were fertile, born at the expected mendelian ratio, and displayed no overt intestinal phenotype (Fig 3A and B). *Kif3a*-deletion was indeed only detectable in intestinal fibroblasts but not epithelial cells (Appendix Fig S1A) and resulted in significantly reduced numbers of PC in the colon of *ColVIcre-Kif3a*$^{flx/flx}$ mice, although the depletion of PC on

Figure 3. Decreased number of primary cilia in colonic fibroblasts promotes CAC.

A, B No alterations in the architecture between colons of *Kif3a*$^{flx/flx}$ (A) and *ColVIcre-Kif3a*$^{flx/flx}$ (B) mice are detectable. Representative images for stains with hematoxylin and eosin, Alcian blue (pH 2.5), Periodic acid–Schiff (PAS), and immunohistochemistry for Ki-67 are shown. Alcian blue stains negatively charged mucopolysaccharides and glycoproteins, whereas PAS recognizes neutral mucopolysaccharides as well. Ki-67-positive cell nuclei were confined to the lower third of the crypts. Scale bars represent 100 μm.

C, D Quantitative analysis of PC expression on vimentin$^+$ (C) and CD140a$^+$ (D) cells in colons of *Kif3a*$^{flx/flx}$ *and ColVIcre-Kif3a*$^{flx/flx}$ mice as described in Fig 2C.

E–I CAC was induced in control (n = 7) and *ColVIcre-Kif3a*$^{flx/flx}$ (n = 7) female mice according to the timeline shown in Fig 2A. (E) Representative images of hematoxylin and eosin staining of paraffin-embedded colon sections. Areas with high-grade dysplasia are delimited by black lines. (F–I) Box-and-whisker plots depicting area (F, G) and number (H, I) of low- and high-grade dysplasia per mouse.

J Kaplan–Meier survival curves of AOM/DSS-treated male *Kif3a*$^{flx/flx}$ (n = 13) and *ColVIcre-Kif3a*$^{flx/flx}$ (n = 11) mice. CAC was induced as described in Fig 2A.

K Quantitative analysis of PC expression on vimentin$^+$ cells in normal colon of *Ift88*$^{flx/flx}$ (n = 7) *and ColVIcre-IFT88*$^{flx/flx}$ (n = 6) mice.

L Kaplan–Meier survival curves of AOM/DSS-treated male *Ift88*$^{flx/flx}$ (n = 11) *and ColVIcre-Ift88*$^{flx/flx}$ (n = 12) mice. Colon carcinogenesis was induced as described in Fig 2A.

Data information: (C, D, G, I, K); n.s. (not significant), *$p < 0.5$, **$p < 0.01$, ****$p < 10^{-4}$ by two-tailed unpaired *t*-test. Scale bar represents 10 mm. (F–I, K) The box plot shows the median (inside line), 25–75 percentiles (box bottom to top), and the Whiskers connect the minimum and the maximum values to the Box.

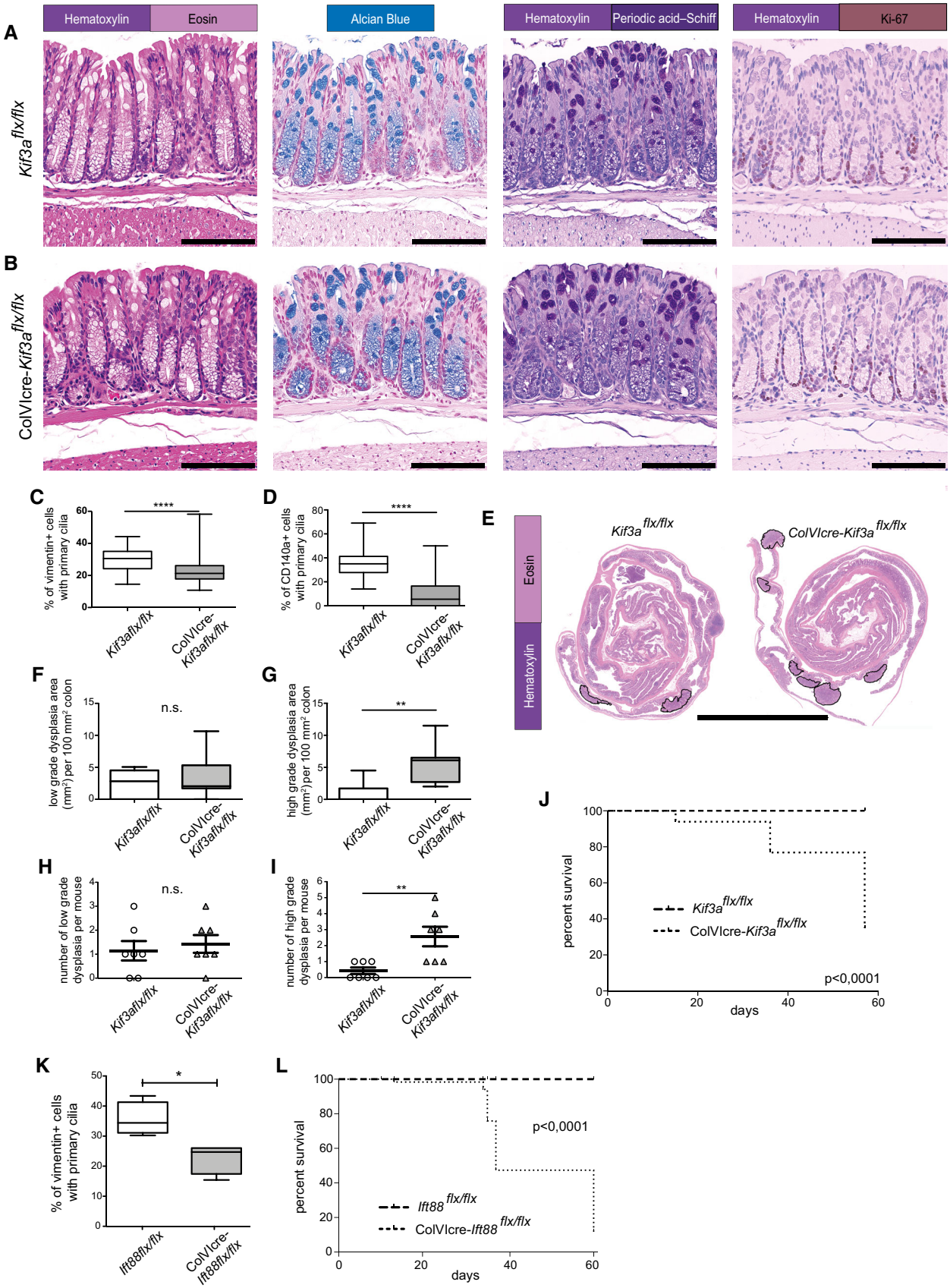

Figure 3.

vimentin^{positive} and CD140a^{positive} colonic fibroblasts was only partial (30–40%, Fig 3C and D). This is in line with a previous report showing that the ColVI promoter is active only in a part of vimentin^{positive} or CD140a^{positive} colonic fibroblasts (Koliaraki *et al*, 2015). Biological and clinical differences between different segments of the murine colon have been described (Minoo *et al*, 2010). The decrease of PC numbers in *ColVIcre-Kif3a*$^{flx/flx}$ mice, however, was consistent across distal, transversal, and proximal regions of the colon suggesting a comparable function of PC in these segments (Appendix Fig S1B).

We next tested whether the reduced number of PC in the colon of *ColVIcre-Kif3a*$^{flx/flx}$ mice alters their susceptibility to AOM/DSS-induced carcinogenesis. Indeed, we found that female *ColVIcre-Kif3a*$^{flx/flx}$ mice displayed an increased incidence of dysplasia, in particular, a higher number of high-grade dysplasia as compared to *Kif3a*$^{flx/flx}$ mice (Fig 3E–I). Male mice are known to be more susceptible to colon carcinogenesis than females (Lee *et al*, 2016), and indeed, following the AOM/DSS treatment, we observed a lower survival rate of about 35% for *ColVIcre-Kif3a*$^{flx/flx}$ males in contrast to 100% of controls (Fig 3J).

Our analysis of *ColVIcre-Kif3a*$^{flx/flx}$ mice revealed a link between PC loss on colonic fibroblasts and AOM/DSS-induced carcinogenesis. To validate these observations, we generated a second mouse model for PC loss in colonic fibroblasts by crossing a conditional knockout allele of the intraflagellar transport protein 88 (*Ift88*$^{flx/flx}$) with *ColVI*cre mice. Similar to Kif3A, Ift88 is essential for cilia assembly and the absence of this protein leads to the loss of PC (Haycraft *et al*, 2007). As expected, *ColVIcre*-mediated deletion of *IFT88* was only detectable in colonic fibroblasts but not epithelial cells (Appendix Fig S2), resulting in decreased numbers of PC in vimentin^{+} colonic cells (Fig 3K). Moreover, male *ColVIcre-Ift88*$^{flx/flx}$ mice showed, similar to *ColVIcre-Kif3a*$^{flx/flx}$ animals, a significantly lower survival rate when exposed to the AOM/DSS colon carcinogenesis protocol (Fig 3L).

Thus, PC deficiency in colonic fibroblasts enhances the sensitivity of mice to colitis-associated carcinogenesis.

Mice deficient for primary cilia are more susceptible to DSS-induced colitis

AOM/DSS-treated *ColVIcre-Kif3a*$^{flx/flx}$ mice displayed an earlier weight loss and significantly lower weight during the first and third treatment of DSS (Fig EV2). Moreover, the male *ColVIcre-Kif3a*$^{flx/flx}$ mice that died during the AOM/DSS protocol manifested severe signs of crypt loss, suggesting to be the cause of death as observed in severe cases of inflammatory bowel disease (Eichele & Kharbanda, 2017). These observations inspired us to test the impact of decreased numbers of colonic PC in inflammation. To this aim, *ColVIcre-Kif3a*$^{flx/flx}$ and control mice were treated for 1 week with DSS (Fig 4A), a commonly used animal model for acute colitis (Wirtz *et al*, 2007; Hao *et al*, 2015). In this model, DSS induces leakiness of the mucosal barrier, allowing infiltration of bacteria and thus initiation of an inflammatory response (Johansson *et al*, 2010). *ColVIcre-Kif3a*$^{flx/flx}$ mice displayed a significantly higher weight loss than *Kif3a*$^{flx/flx}$ mice at days 7, 8, and 9 after the start of the protocol (Fig 4B and C). Concurring with the more pronounced weight loss, colons of *ColVIcre-Kif3a*$^{flx/flx}$ mice displayed larger areas of architectural irregularities and crypt loss (Fig 4D–F). Notably, 4 out of 7 *ColVIcre-Kif3a*$^{flx/flx}$ mice showed signs of dysplasia, whereas none of the control animals exhibited signs of dysplasia (Fig 4G). Moreover, *ColVIcre-Kif3a*$^{flx/flx}$ mice displayed an increased presence of F4/80^{positive} macrophages in areas with crypt loss (Fig 4H), whereas numbers of Gr-1^{positive} granulocytes, B220^{positive} B cells, and CD3^{positive} T cells were unaltered (Fig EV3).

Figure 4. PC-deficient mice are more susceptible to DSS-induced colitis.

A Experimental timeline for DSS-induced colitis in control (n = 7) and *ColVIcre-Kif3a*$^{flx/flx}$ (n = 7) male mice.

B, C Relative weight development in DSS-treated mice represented as % of relative weight loss (B) and the area under the curve (AUC) for the relative weight development (C). Individual body weight at the start of the protocol was taken as 100%. (B) Error bars represent standard deviation. *$p < 0.05$ by two-tailed unpaired t-tests. (C) The AUC was calculated for each mouse and compared between the two cohorts of mice. The box plot shows the median (inside line), 25–75 percentiles (box bottom to top), and the Whiskers connect the minimum and the maximum values to the Box.

D–F At the end of the protocol described in (A) mice were sacrificed and colons were analyzed by histology for colitis severity including areas of irregular crypts (i.e., nonparallel crypts, variable crypt diameters, bifurcation and branched crypts; D, E) and crypt loss (i.e., mucosa devoid of crypts; D, F). Data are presented as Box-and-whisker plots. *$p < 0.05$ by two-tailed unpaired t-test. Scale bar represents 1.5 mm.

G Incidence of dysplasia in DSS-treated *ColVIcre-Kif3a*$^{flx/flx}$ mice. Low- and high-grade dysplasia was identified as described in Fig 2B.

H Elevated numbers of F4/80^{+} macrophages in colons of DSS-treated *ColVIcre-Kif3a*$^{flx/flx}$ mice. Representative images for F4/80 staining in areas with crypt loss are shown. At least five fields in the regions of crypt loss were analyzed from each colon of control (n = 6) and *ColVIcre-Kif3a*$^{flx/flx}$ (n = 6) mice. Mean cell numbers were scored as low (< 500 cells/mm^2) or high (> 500 cells/mm^2). Scale bar represents 250 µm.

K Quantitative analysis of PC expression on vimentin^{+} cells in normal colon of *Ift88*$^{flx/flx}$ (n = 7) and *ColVIcre-IFT88*$^{flx/flx}$ (n = 6) mice. *$p < 0.05$ by two-tailed unpaired t-test.

I, J Weight development in DSS-treated *ColVIcre-Ift88*$^{flx/flx}$ (n = 6) and control (n = 7) mice following the indicated timeline. Shown are relative weight loss in % (I) and the AUC for the relative weight development (J). For the statistical analysis see (B, C).

K, L At the end of the protocol described in (I) mice were sacrificed and colons were analyzed for length (K), and crypt loss (L). Data are presented as Box-and-whisker plots. **$p < 0.01$ by two-tailed unpaired t-test.

M Comparison of primary cilia numbers on vimentin^{positive} cells in colons of untreated and DSS-treated wild type mice. DSS treatment was performed as illustrated in (A). Primary cilia in DSS-treated mice were depicted in areas of regeneration (14 fields in average 0.250 mm^2). Significance values were determined by two-tailed unpaired t-tests (**$p < 10^{-2}$).

N Decreased number of PC in inflamed tissue of patients with ulcerative colitis. Shown are the results of matched-pair analysis for PC expression per vimentin^{+} cells as an arbitrary unit (AU, see Materials and Methods). The lines link values obtained for regions of ulceration in the ileum with those of normal regions from the same patient, demonstrating the difference in each pair.

Data information: (E, F, J–M): *$p < 0.05$, **$p < 0.01$, ****$p < 10^{-4}$ by two-tailed unpaired t-test; (N): *$p < 0.05$ by paired t-test. (C, E, F, J–M). The box plot shows the median (inside line), 25–75 percentiles (box bottom to top), and the Whiskers connect the minimum and the maximum values to the Box.

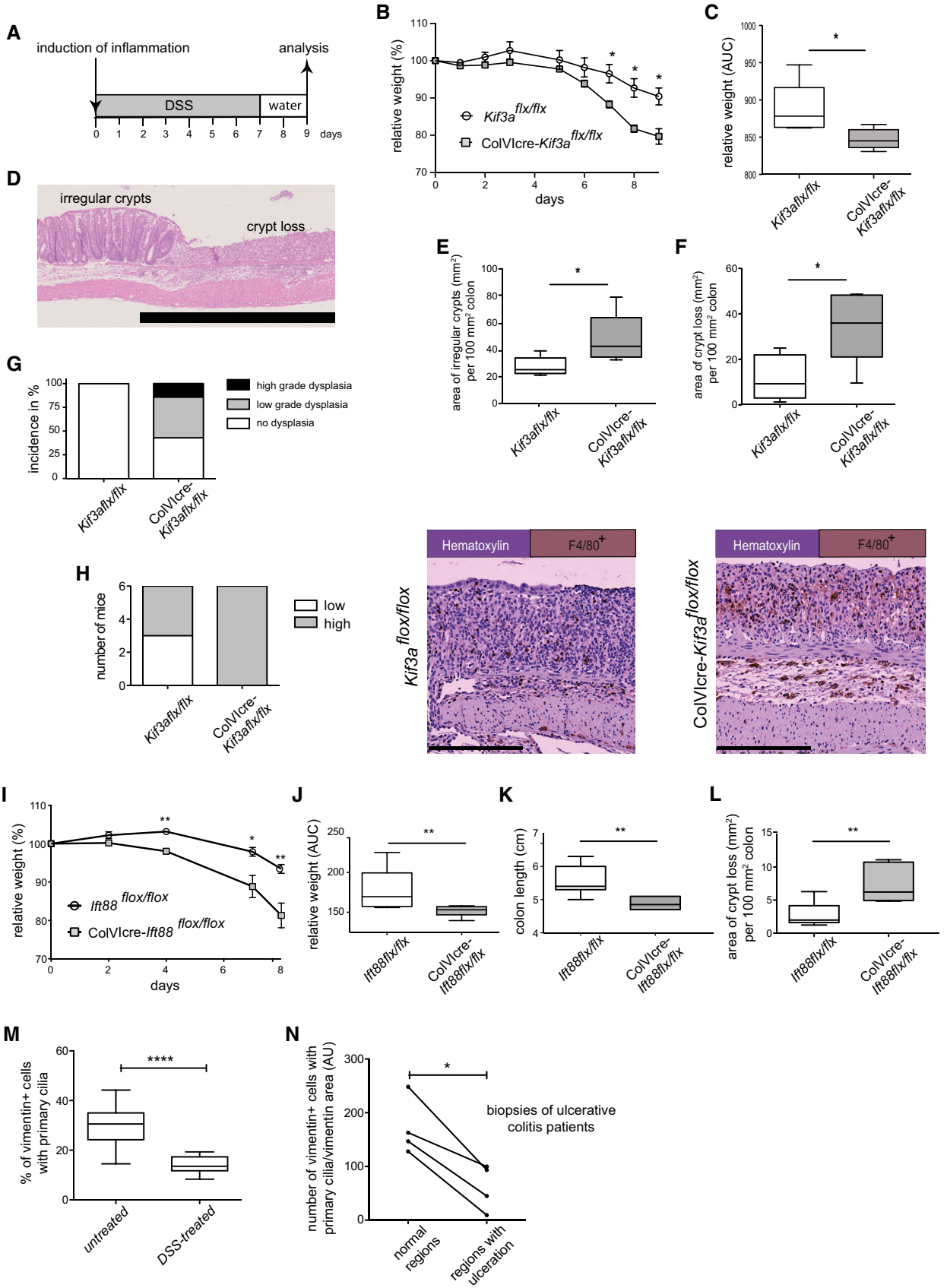

Figure 4.

To confirm that the increased susceptibility of *ColVIcre-Kif3a*$^{flx/flx}$ mice relates to PC deficiency we exposed *ColVIcre-Ift88*$^{flx/flx}$ animals to DSS-induced colitis. Indeed, these developed more severe signs of acute colitis compared with control animals, as manifested by elevated weight loss, decreased colon length, and increased crypt loss (Fig 4I–L).

Consistent with the increased susceptibility of PC-deficient mice to DSS-induced colitis we detected decreased numbers of PC on colonic fibroblasts during acute colitis compared with those of untreated mice further underpinning a link between the presence of PC and intestinal inflammation (Fig 4M). Strikingly, we also detected decreased numbers of PC in regions of inflamed tissue from patients with ulcerative colitis, when compared to neighboring normal tissue (Fig 4N).

DSS-treated colons of PC-deficient mice display elevated IL-6 signaling

To gain insight into the molecular traits modulated by PC presence, we generated conditioned medium from distal colons taken from DSS-treated control and *ColVIcre-IFT88*$^{flx/flx}$ animals and analyzed those by mass spectrometry employing LC-QTOF-MS/MS analysis (Fig 5A). The supervised analysis identified 392 and 424 proteins in medium from DSS-treated colons of control and *ColVIcre-IFT88*$^{flx/flx}$ mice, respectively (ProteomeXchange identifier pxd033440). Ingenuity Pathway Analysis revealed a prominent elevated activation of IL-6 as well as the connected EGF signaling (Schumacher & Rose-John, 2019) in DSS-treated colon of *ColVIcre-IFT88*$^{flx/flx}$ mice (Fig 5B and ProteomeXchange pxd033440).

Given that a critical role for the prototypic pro-inflammatory cytokine IL-6 in DSS-induced colitis is well established (Chassaing *et al*, 2014) and concurring with the secretome analysis, we detected elevated *Il-6* transcript levels in distal colons from DSS-treated *ColVIcre-Kif3a*$^{flx/flx}$ mice as compared to controls (Fig 5C). Macrophages can be an important source of IL-6 (Naito *et al*, 2004) and a higher number of F4/80^{positive} macrophages in areas with crypt loss from DSS-treated *ColVIcre-Kif3a*$^{flx/flx}$ mice showed detectable IL-6 expression by immunofluorescence on tissue sections (Fig 5D). In addition, fibroblasts and epithelial cells can be also significant producers of IL-6 (Waldner *et al*, 2012), and in DSS-treated *ColVIcre-IFT88*$^{flx/flx}$ mice both displayed an elevated production of IL-6 as determined by immunofluorescent analysis of colons (Fig 5E upper panel). Taken together, the increased susceptibility of PC-deficient mice to chemically induced colitis is associated with elevated IL-6 response. A prime target of IL-6 is the transcription factor *Stat3* (Karin & Clevers, 2016; Taniguchi *et al*, 2017), and indeed, we detected higher levels of nuclear phospho-Stat3 in vimentin^{positive} fibroblasts (Fig 5E lower panel).

IL-6 suppresses PC formation on colonic fibroblasts

To study the relationship between an inflammatory environment and PC presence on colonic fibroblasts (CF), we studied primary CF cultures after two passages (termed 2P-CF, see Fig 6A). In these cultures, ciliogenesis was reproducibly induced in 30–40% of cells by 24 h of starvation (Fig 6B, control condition, and Fig EV4A and B). Notably, in fibroblast cultures derived from *ColVIcre-IFT88*$^{flx/flx}$ mice, only about 10% of the cells displayed PC upon starvation (Fig EV4A and B). Thus, the 2P-CF cultures plus starvation mimic the *in vivo* proportion of PC on CF in an intact colon and thus allow to explore the biology of PC. We generated conditioned starvation medium from colons of DSS-treated (termed inflammatory conditioned medium, inf-CM) and -untreated control animals (termed control conditioned medium, co-CM) and cultured 2P-CF in those media for 24 h. 30–40% of 2P-CF starved in the control medium displayed PC, whereas the PC number on 2P-CF starved in inf-CM was consistently lower (Fig 6B). We performed RNA-seq analysis of 2P-CF starved in inflammatory or in control medium to gain insight into the molecular traits of those cell cultures. Supervised analysis revealed 782 genes differentially regulated between two starvation conditions: 479 genes were upregulated (cluster 1) and 303 genes were downregulated (cluster 2) in the inflammatory condition compared with the control condition (Fig 6C and GEO ID GSE207877). The top discriminant transcripts in the control setting included genes related to epithelial-mesenchymal transition (EMT) and Hedgehog canonical and noncanonical signaling, whereas those in the inflammatory condition included prominently genes associated with inflammatory response (GEO ID GSE207877). The gene expression signature was then submitted to Gene Set Enrichment Analysis (GSEA) (http://www.broadinstitute.org/gsea/), in regard to the 50-hallmark gene sets from the Molecular Signatures Database (MSigDB). Strikingly, the most significantly upregulated pathway in the inflammatory condition was the IL-6-JAK-STAT3 gene set (Fig 6D). In addition, the inflammatory condition upregulated the *Il-6* transcript itself in the fibroblast cultures (GEO ID GSE207877), highlighting an active inflammatory loop.

Figure 5. DSS-treated colons of PC-deficient mice display elevated IL-6 signaling.

A Preparation of conditioned medium. Colons were taken from DSS-treated (7 days) *Ift88*$^{flx/flx}$ (n = 6) and *ColVIcre-IFT88*$^{flx/flx}$ (n = 6) mice and kept for 4 h in PBS.

B Graphical summaries of IPA pathway analysis of proteins identified by shotgun proteomics of conditioned media generated as described in (A). Nodes significantly upregulated (orange) and downregulated (blue) in the conditioned medium prepared as described in (A).

C Transcript levels of Il-6 in DSS-treated *Kif3a*$^{flx/flx}$ and *ColVIcre-Kif3a*$^{flx/flx}$ mice (according to the protocol shown in Fig 4A). Three independent mRNA samples were analyzed by RT–qPCR, and mean values standardized to the expression of the housekeeping gene *Tbp* are shown. Error bars represent SEM.

D Elevated numbers of IL-6-expressing F4/80^{+} macrophages in *ColVIcre-Kif3a*$^{flx/flx}$ mice treated with DSS as described in Fig 4A. At least five fields in the regions of crypt loss were analyzed. Scale bar represents 100 μm. *$p < 0.05$ was calculated by the chi-squared test.

E Elevated IL-6 expression in colonic epithelial cells and fibroblasts of PC-deficient mice upon DSS treatment as described in Fig 4A. Representative images and corresponding quantification of vimentin^{positive} fibroblasts (in green) and vimentin^{negative} epithelial cells (identified by histological criteria) labeled for IL-6 (upper panel) and p-STAT3 (lower panel) in red. Nuclei were stained with DAPI (in blue). White arrowheads indicate IL-6 (upper panel) and nuclear staining for pSTAT3 (lower panel) for vimentin^{positive} fibroblasts, blue arrowheads the respective labeling for epithelial cells. Scale bars represent 100 μm. *$p < 0.05$, ****$p < 10^{-4}$, n.s. (not significant) was calculated by the chi-squared test on absolute numbers and is presented as % of cells positive for the indicated marker within vimentin^{positive} and epithelial cells, respectively.

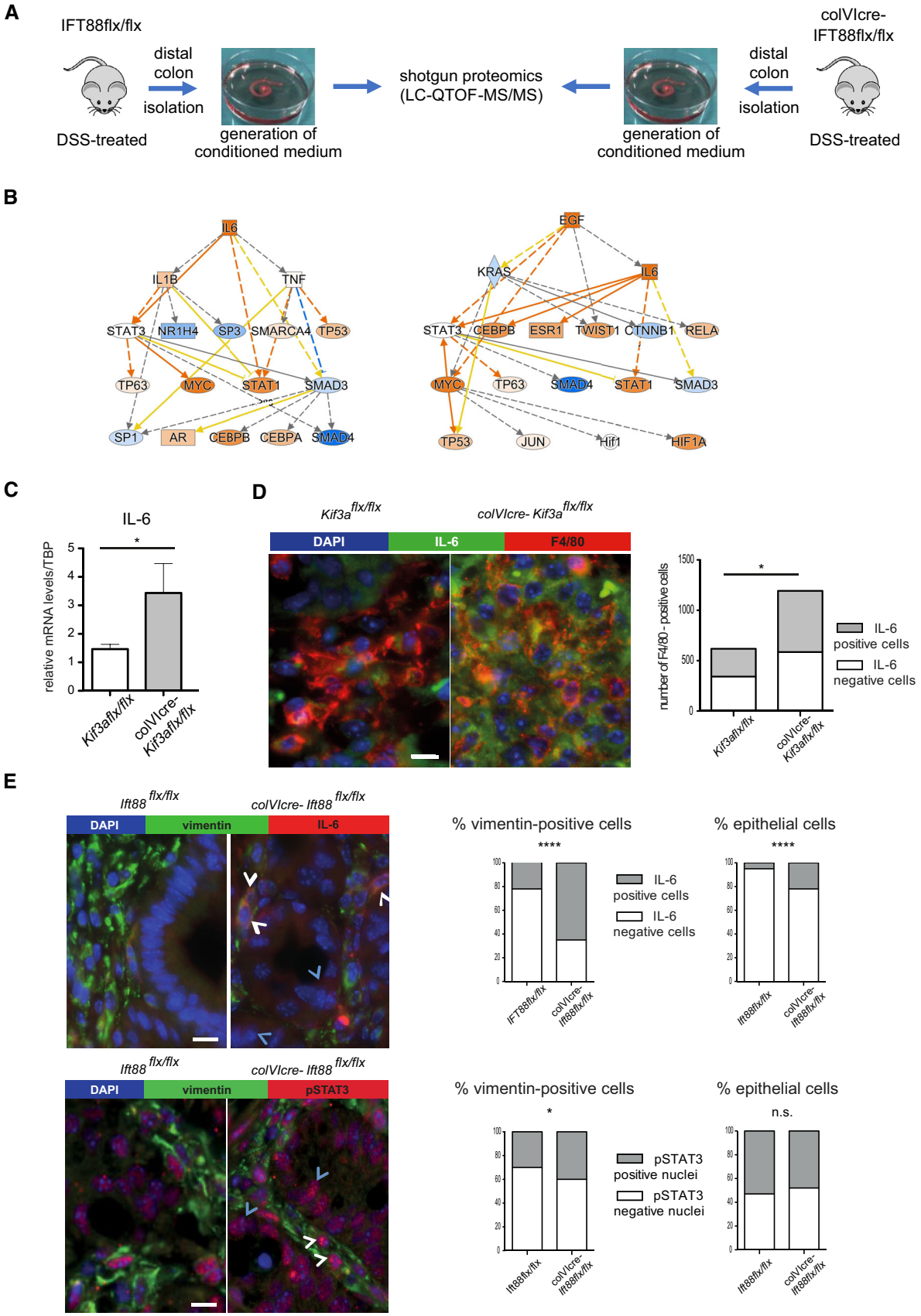

Figure 5.

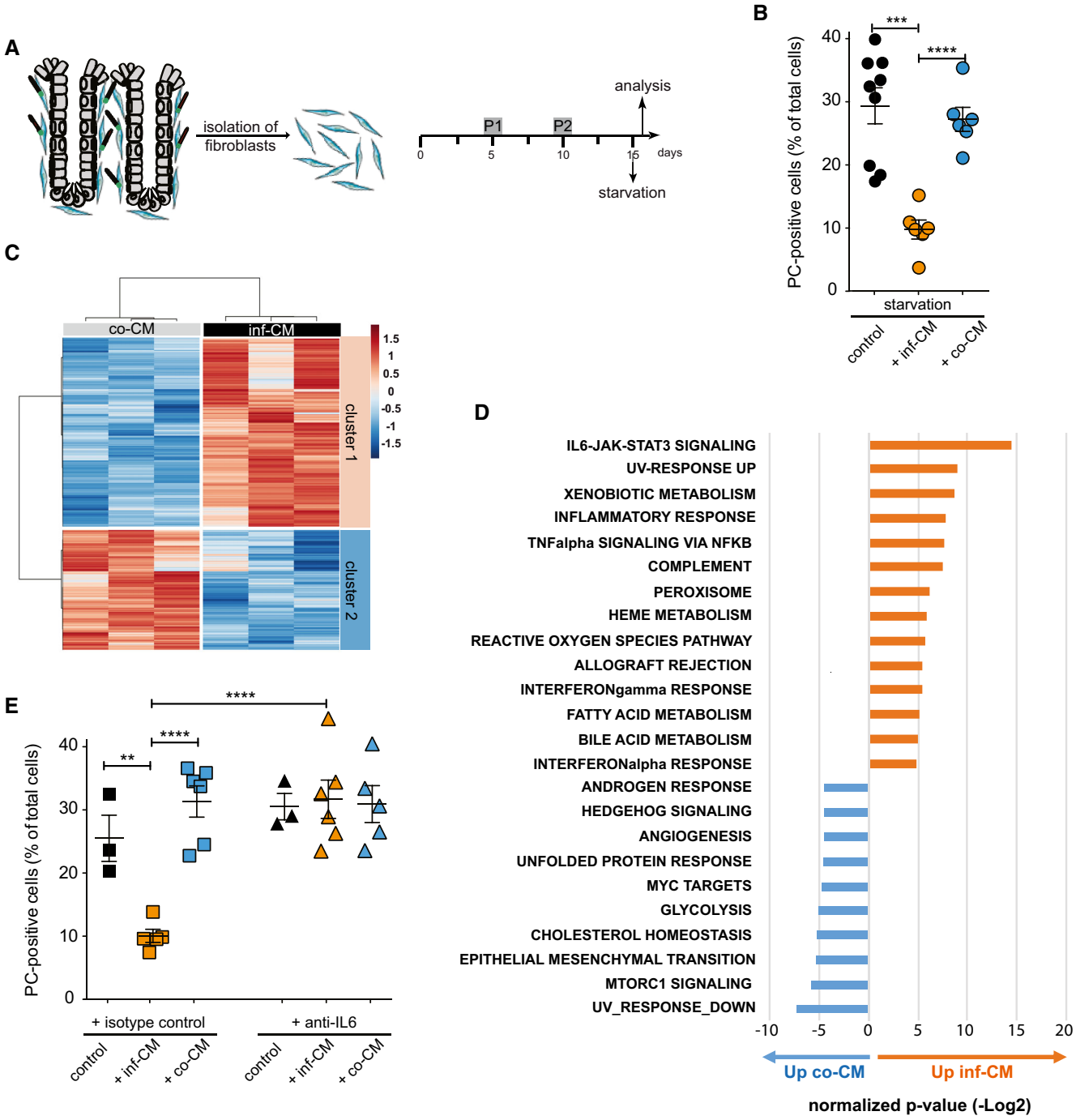

Figure 6. IL-6 suppresses PC formation on colonic fibroblasts (CF).

A Generation of primary CF cultures from *Ift88*$^{fix/fix}$ mice, that is, control animals. CF were isolated as described in the Materials and Methods section and passaged twice (2P-CF) at days 5–7 (P1) and 9–11 (P2), and exposed to starvation at day 15 after isolation.

B Starvation in the presence of inflammatory conditioned medium (inf-CM) prevents PC formation on 2P-CF, as observed in starvation medium (PBS, 0.5% BSA) and control conditioned medium (co-CM). Conditioned media were generated from 4 h cultures of colons isolated from DSS-treated (inf-CM) and untreated (co-CM) mice (n = 6). Error bars represent standard deviation.

C Heat map of paired RNA-seq analysis of 2P-CF treated with either co-CM (n = 3) or inf-CM (n = 3) displaying two distinct clusters.

D Analysis of gene expression signatures revealed the IL-6/Jak/Stat3 pro-inflammatory core gene set as the most elevated one in inf-CM treated cells.

E Blocking of Il-6 abrogates the PC-dampening effect of inf-CM on 2P-CF. Cells were treated for 24 h in starvation medium (control), inf-CM, or co-CM in the presence of antagonistic Il-6 antibody or isotype control (5 μg/ml each). Error bars represent standard deviation.

Data information: (B, E) Significance values were determined by two-tailed unpaired t-tests (n = 5; *$p < 0.05$, **$p < 10^{-2}$, ***$p < 10^{-3}$, ****$p < 10^{-4}$).

Importantly, the ciliogenesis-dampening effect of the inflammatory medium was reverted by the addition of an antagonistic anti-IL-6 antibody in the conditioned medium from the DSS-treated colon (Fig 6E). Altogether, IL-6 signaling appears to be one of the dominant pathways triggering PC loss on colonic fibroblasts in an inflammatory context.

Decreased numbers of PC in human CRC biopsies

To investigate whether PC are also present in human colons, we performed an IHC analysis of three biopsies of healthy donors. Indeed, PC were detectable mostly on vimentin^{positive} fibroblasts in the lamina propria and only on few epithelial cells (Figs 7A and EV5A and B). We next analyzed the presence of PC on tumor tissues of 28 CRC patients at different stages of the disease. Sections of tumor tissues of all four stages harbored decreased numbers of PC on vimentin^{positive} colonic fibroblasts compared with the respective peritumoral region as well as normal colon (Fig 7B). Of note, the tissue sections of the stage 4 samples did not contain adjacent normal tissue and were thus compared with the mean calculated from the analysis of peritumoral tissue of stage 1–3 patients. Moreover, we noted that vimentin^{positive} regions were enlarged in the tumoral as compared to the peritumoral regions of several samples. Hence, we analyzed PC expression in regions containing exclusively vimentin^{positive} cells to convey a more unbiased approach. Notably, the latter analysis confirmed the decreased number of PC in tumors compared with peritumoral areas (Fig 7C).

Discussion

Defects in primary cilia (PC) are best understood for inherited genetic disorders, so-called ciliopathies. While the role of PC in other pathologies is emerging, and various reports associate PC with carcinogenesis, their role in tumor development appears to vary between different types of cancers. Reduced numbers of PC have been described for breast and pancreatic cancer, as well as melanoma (reviewed in Eguether & Hahne, 2018; Liu *et al*, 2018), whereas PC were reported to be maintained in about half of the tested biopsies of medulloblastoma and basal cell carcinoma (BCC) patients. This dichotomy is underlined by the observation in mouse models that, depending on the nature of the initiating oncogenic event, cilia ablation facilitates or blocks medulloblastoma as well as BCC tumor formation (Han *et al*, 2009; Wong *et al*, 2009).

In this study, we investigated the role of PC in colonic pathology, i.e., colon carcinogenesis and colitis. We found that the numbers of PC decrease not only during colon carcinogenesis but also during acute colitis in mice. Intriguingly, these findings in mice concur with the decreased number of PC detected in tumor areas of CRC patients as well as in inflamed tissue areas of patients with ulcerative colitis, when compared to neighboring normal tissue. In line, a previous report described a correlation between the frequency of colonic PC and disease outcomes in CRC patients (Dvorak *et al*, 2016). The authors found a significantly longer overall survival of CRC patients with a higher frequency of PC in the colon, concurring with our observations in mice. Nevertheless, this study did not assess which cells in the colon express PC.

Here we report that mostly fibroblasts carry PC in murine as well as the human colon. To investigate the consequences of PC loss in colonic fibroblasts, we crossed the two commonly used mouse strains to study PC, i.e., *Kif3a*$^{flx/flx}$ and *Ift88*$^{flx/flx}$, to *ColVIcre*-transgenic mice, targeting mesenchymal cells including subsets of colonic fibroblasts (Armaka *et al*, 2008; Koliaraki *et al*, 2015). Accordingly, the number of PC was significantly lower in colons of both *ColVIcre-Kif3a*$^{flx/flx}$ and *ColVIcre-Ift88*$^{flx/flx}$ mice compared with control animals, which did not perturb the colonic architecture. However, *ColVIcre-Kif3a*$^{flx/flx}$ as well as *ColVIcre-IFT88*$^{flx/flx}$ animals displayed increased susceptibility to chemically induced colitis and colitis-associated colon carcinogenesis. These findings reveal, to our best knowledge for the first time, an impact of deregulated PC presence on colonic fibroblasts in intestinal pathology. In addition to their role in PC formation, KIF3a and IFT88 may promote cilia-independent functions, such as spindle orientation or mother centriole appendage formation (Delaval *et al*, 2011; Kodani *et al*, 2013). Therefore, we decided to study both mutant mice deficient in PC to allow a conclusion of whether a potential phenotype is truly cilia-dependent. The complementary results obtained in *ColVIcre-Kif3a*$^{flx/flx}$ and *ColVIcre-Ift88*$^{flx/flx}$ animals allow concluding that decreased PC numbers are at their origin.

Crucial in the regulation of intestinal homeostasis and pathology is the crosstalk between epithelium lining the crypts and neighboring fibroblasts, which are characterized by a remarkable heterogeneity and the capacity to differentiate into functionally distinct subsets (Koliaraki *et al*, 2020; Onfroy-Roy *et al*, 2021). Different morphogenetic pathways participate in the epithelium-fibroblast crosstalk, such as Wnt signaling through the secretion of factors from adjacent fibroblasts, which is essential in the maintenance of the epithelial stem cell compartment at the bottom of crypts (Medema & Vermeulen, 2011). Particularly relevant to our findings is a study demonstrating that activated stromal hedgehog signaling can suppress colon carcinogenesis (Gerling *et al*, 2016), as hedgehog signaling depends on PC presence (Eguether & Hahne, 2018; Liu *et al*, 2018).

Figure 7. Decreased number of primary cilia in tumoral tissues of CRC patients compared with peritumoral regions.

A Representative image of vimentin^{+} fibroblasts (in green) expressing PC (identified using Arl13b, in red) in a normal colon. Nuclei were stained with DAPI (in blue). Most PC are detected on vimentin^{+} cells (arrow), and few on vimentin-negative epithelial cells (arrowhead). Scale bars represent 50 μm in the upper and 10 μm in the lower panel.

B, C Quantitative analysis of PC presence on tumoral and peritumoral regions of colons from CRC patients (n = 28) at tumor (T) stages 1–4. The panels represent the quantification of PC expression (B) of vimentin^{positive} cells per mm^2 and (C) per vimentin^{positive} cells as an arbitrary unit (AU, see Materials and Methods). Data are presented as Box-and-whisker plots. The box plot shows the median (inside line), 25–75 percentiles (box bottom to top), and the Whiskers connect the minimum and the maximum values to the Box. *$p < 0.05$, **$p < 0.01$, ***$p < 10^{-3}$, ****$p < 10^{-4}$ by two-tailed unpaired t-test. Images were acquired on an Andor Dragonfly Spinning Disk Confocal microscope and analyzed with the Imaris software. Quantification of PC and Vimentin^{+} fibroblasts was done on at least five random fields (about 1 mm^2 each) per sample using ImageJ software.

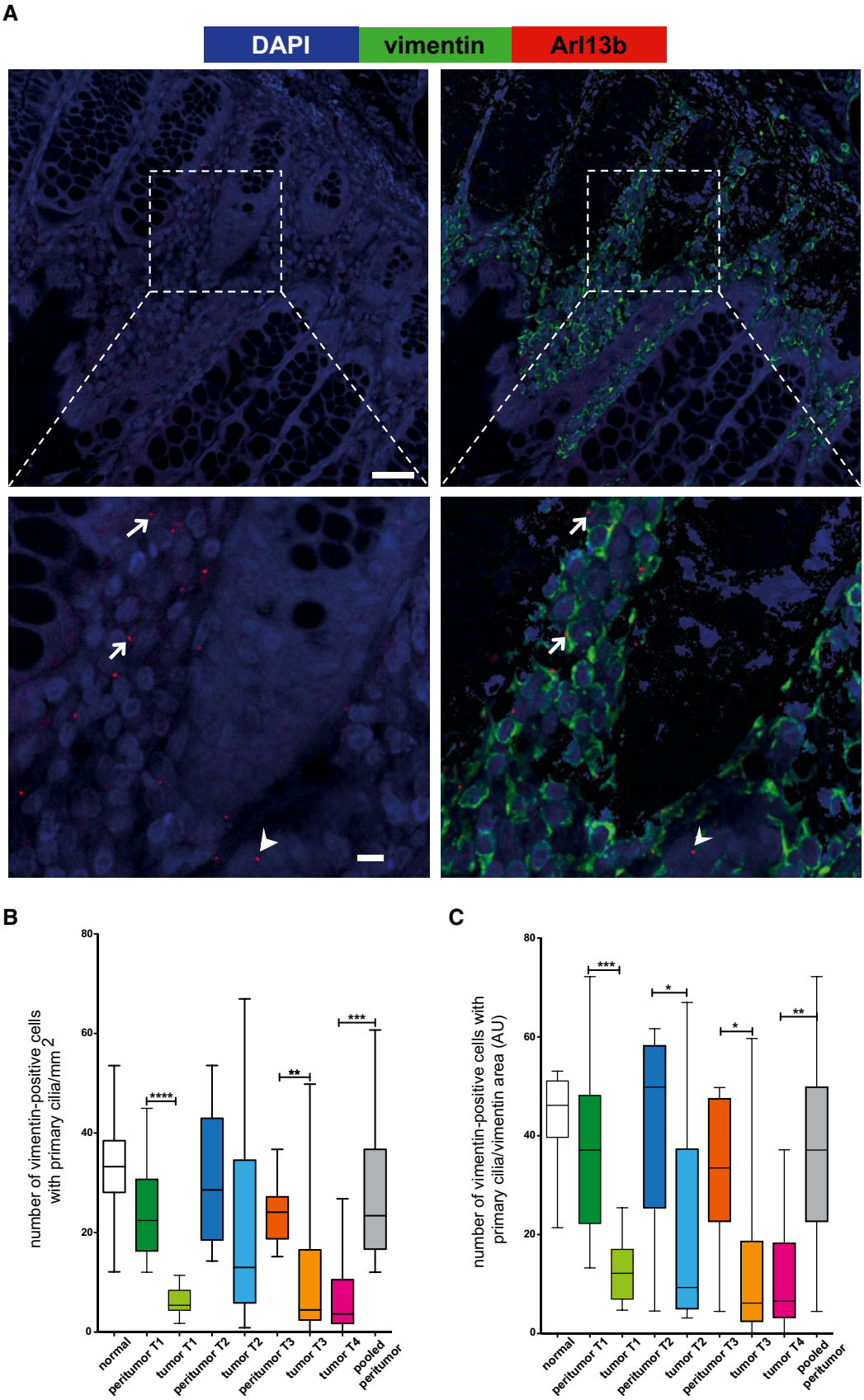

Figure 7.

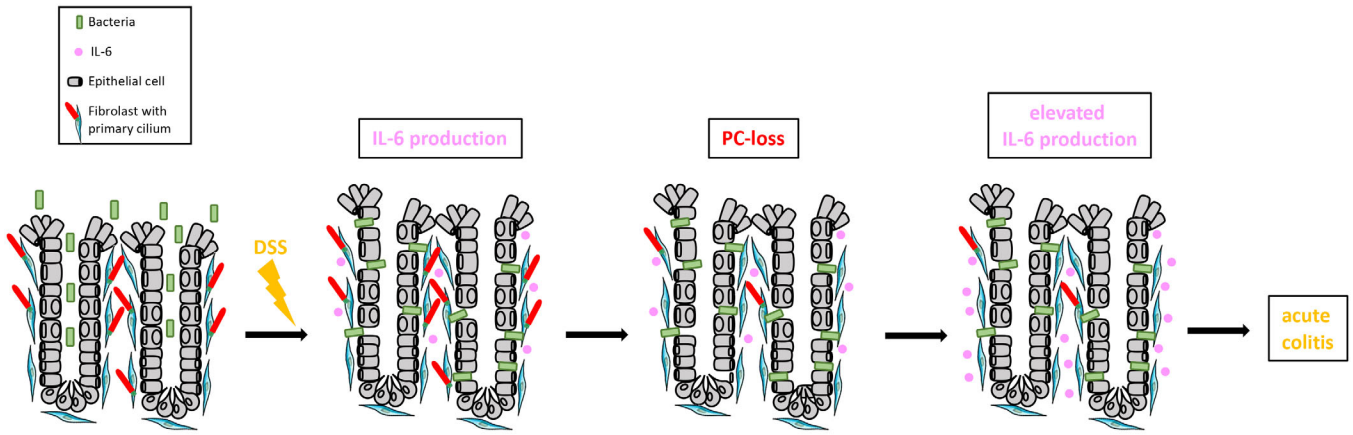

Figure 8. Loss of PC amplifies colonic inflammation.

DSS is toxic to the mucosal epithelial cells specifically in the colon, but not genotoxic, leading to the destruction of the mucosal barrier. Our data suggest that the initial inflammation caused by bacteria penetrating the mucosal barrier is promoted by an amplification loop between PC loss and IL-6 production. This circuit appears to be enhanced in mice deficient for PC.

Indeed, our RNA-seq analysis of primary CF displayed a downregulation of Hedgehog signaling in inflammatory medium-treated cells, which have lower PC numbers (Fig 6D and GEO ID GSE207877).

The respective RNA-seq analysis, however, identified IL-6 signaling as the most significantly upregulated pathway in the inflammatory condition. Strikingly, an antagonistic anti-IL-6 antibody blocked the PC-suppressing effect of the inflammatory medium in primary fibroblast cultures. Moreover, secretome analysis displayed elevated IL-6 levels in the inflamed colons of PC-deficient mice. This concurs with the expression levels of IL-6 detected in different cellular compartments of colitic colons by immunohistochemistry. We therefore propose a model, in which PC loss promotes the response of DSS-induced inflammation through an amplification loop of IL-6 upregulation and PC loss during colitis as illustrated in Fig 8. This circuit is initiated by the DSS-induced breakdown of the mucosal barrier enabling the entry of luminal bacteria. Reports associating PC alterations with inflammation in pathologies besides ciliopathies are still limited. One example is a study describing that the removal of endothelial PC promotes atherosclerosis in mice that correlated with an increased expression of IL-6 (Dinsmore & Reiter, 2016), thus concurring with our observations.

Inflammation is an important driver in the regeneration of damaged tissue, by inducing hyperproliferation of epithelial tissue triggered by pro-inflammatory cytokines such as IL-6 (Kuhn *et al*, 2014; Karin & Clevers, 2016). However, excessive production of pro-inflammatory cytokines, can also be deleterious and promote tumor formation (Todoric *et al*, 2016). Indeed, we observed an increased incidence of dysplasia in DSS-treated *ColVIcre-Kif3a*$^{flx/flx}$ mice. DSS is not genotoxic, but intestinal inflammation was shown to induce DNA damage and thus promoting dysplasia (Westbrook *et al*, 2009). Therefore, the augmented inflammatory response in DSS-treated *ColVIcre-Kif3a*$^{flx/flx}$ mice appears to be at the origin of the observed dysplasia. This together with our finding that PC numbers progressively decrease during the transition from normal tissue to low-grade and then high-grade dysplasia suggests the use of PC presence as an early biomarker.

Taken together, decreased numbers of PC on colonic fibroblasts in mice have no consequence in physiological steady-state conditions but enhance the inflammatory response in acute colitis and amplify chemically induced colitis-associated colon carcinogenesis. The observations made in mice concur with the corresponding human pathologies, i.e., colitis and CRC, as those display decreased numbers of PC on intestinal fibroblasts. Our findings support a model, in which PC loss plays a disease-promoting role in colonic pathology.

Materials and Methods

All analyses were performed in a blinded manner.

Animal experimentation

Mouse experiments were performed in strict accordance with the guidelines of the European Community (directive n°2010/63/EU) and the French National Committee (Project number APAF IS#18685) for the care and use of laboratory animals. The latter includes a statistical analysis to minimize the number of mice to be used for identifying significant differences. To study PC, we used *Kif3a*$^{flx/flx}$ and *Ift88*$^{flx/flx}$ mice, which have been previously described (Marszalek *et al*, 1999; Haycraft *et al*, 2007). Tissue-specific knockout mice were obtained by crossing with *ColVIcre*-transgenic strain. The latter was obtained by G. Kollias (Armaka *et al*, 2008; Koliaraki *et al*, 2015). Mice were maintained on C57BL/6 genetic background, and experimental groups contained littermates that were caged together according to gender. Genotyping was done as described before (Marszalek *et al*, 1999; el Marjou *et al*, 2004; Haycraft *et al*, 2007; Armaka *et al*, 2008). *ColVIcre-Kif3a*$^{flx/flx}$ and *ColVIcre-Ift88*$^{flx/fl}$ mice were fertile, born at the expected Mendelian ratio, and displayed no overt intestinal phenotype. Mice used for the experiments described were used at age of 8–12 weeks.

Patient samples

Formalin-fixed and paraffin-embedded CRC samples of different histological grades were obtained from the institutional biobank of the University Hospital of Liege, Belgium following the approval of the Institutional Ethics Committee No. 2009/69. According to Belgian law, informed consent was not necessary because all patients are informed that their residual surgical material can be used for research unless they opt out. Details of CRC samples obtained from the University Hospital (CHU) of Liège are listed in Appendix Table S1. The cohort of patients with ulcerative colitis from the Hospital Saint-Antoine (Paris) was declared under the number #CNIL1104603 and all patients (two men, 38 and 43 years old, and two women, 25 and 57 years old) gave consent to this research.

Histology and immunohistochemistry

Organs were fixed in 10% neutral buffered formalin (NBF) solution for 24 h. Histological examination was performed on paraffin-embedded sections stained with hematoxylin and eosin. Immunohistochemistry was performed on formalin-fixed and paraffin-embedded tissues cut into 4-µm sections. After blocking of nonspecific binding (with TBS-10% goat serum-5% BSA-5% milk-0.3% triton), samples were incubated with primary antibody (see Appendix Table S2) for 1 h at room temperature or overnight at 4°C and avidin/biotin complex or polymer horseradish peroxidase kits for primary mouse or rabbit antibodies (Vector Laboratories) were used for detection. For immunofluorescence analysis, samples were incubated with primary antibodies for 1 h and revealed with fluorescent-labeled secondary antibodies (Vector Laboratories). DNA was stained using 20 µg/ml of 4',6'-diamidino-2-phenylindole (DAPI). For the detection of PC, we followed a previously described protocol that allows the detection of PC on paraffin-embedded tissue (Coy *et al*, 2016).

DSS-induced colitis and colitis-associated carcinogenesis (CAC)

To induce colitis, 8–12 week-old mice were treated for 7 days with 2.5% (w/v) dextran sodium sulfate (DSS; TdB Sweden) added to the drinking water. Mice were sacrificed at indicated time points. The weight of the mice was daily followed and in case weight loss was more important than 20% mice were sacrificed. For colitis-associated carcinogenesis, mice were intraperitoneally injected with azoxymethane (AOM, 6.5 µg/g of body weight), followed by three cycles of 2.5% (w/v) DSS administered in the drinking water (Fig 2A). In between the cycles the mice received no treatment for 2 weeks. For histological analysis, the entire colon was flushed, rolled, and fixed with NBF solution and embedded in paraffin. Tissue sections (4 µm) were stained with hematoxylin and eosin, Alcian blue, or processed for IHC after deparaffinization and subsequent incubation with the primary antibodies listed in Appendix Table S2. Histological grading of AOM/DSS-induced tumors was determined with a blinded genotype according to the described classification of intestinal neoplasia (Washington *et al*, 2013).

Cell culture

The protocol for the isolation of colonial fibroblasts (CF) was modified according to Roulis *et al* (2014). Briefly, colons were isolated from mice, flushed with PBS, and then opened longitudinally and processed as follows. Intestinal pieces were cut into small pieces and incubated in EDTA-containing buffer (HBSS/2% FCS/5 mM EDTA) at 37°C for 20 min under continuous shaking to release colonic epithelial cells (CEC). After extensive washes, the tissue was further processed by treatment with 62.5 µg/ml Liberase and 40 µg/ml DNAse (Sigma) in HBSS/2% FCS for 50 min at 37°C under continuous shaking to isolate CF. Cells were filtered through a 70-µm strainer, washed with PBS, and subsequently analyzed or taken in culture. CF was cultured in DMEM/10%FCS for 2 passages (2P-CF). To induce the formation of PC, 70–90% confluent 2P-CF was cultured for 24 h in a starvation medium containing 1% BSA. In specific experiments, cells were cultured in the presence of inflammatory (inf) or control (co) conditioned medium (CM). To obtain those, colons were isolated from control mice and animals treated for 7 days with DSS, washed with PBS, and subsequently took in culture for 4 h in the medium. For blocking experiments, 5 µg/ml of antagonistic anti-IL-6 antibody MP5-20F3 and isotype control (rat IgG1) were used (both Biolegend).

Microscopy and imaging

Histological slides were scanned using Nanozoomer 2.0 HT scanner with a 40× objective and visualized with NDP.view2 viewing software (Hamamatsu). Fluorescent images were acquired on a brightfield microscope (Leica) using Metamorph software, inverted Confocal SP5 (Leica) using the Leica LAS AF software, or an Andor Dragonfly Spinning Disk Confocal microscope employing Imaris software. Quantification of PC and vimentin^{positive} fibroblasts was done on at least five random fields (about 1 mm^2 each) per sample using Imaris and ImageJ software. Images were processed with ImageJ. Images were assembled and adjusted with Adobe Photoshop/ Illustrator. Counting of PC was performed using z-stack acquisition. Co-staining with cell markers was confirmed on distinct layers. In analyses of human biopsies, PC numbers were calculated either per mm^2 or per Vimentin-stained area using an arbitrary unit (AU corresponding to 10,000 square pixel) of vimentin^{positive} cells.

Label-free proteomics

To analyze the secretome of colitic colons, shotgun proteomics analyses were performed, accordingly with methods we described before (Pieragostino *et al*, 2019). Colons were isolated from *ColVIcre-Ift88$^{flx/flx}$* and control mice (n = 6 each) and kept in culture for 4 h. Supernatants were assayed for protein concentration through Bradford assay (Bio-Rad, Hercules, CA, USA) using Bovine Serum Albumin (BSA, Sigma-Aldrich, St. Louis, MI, USA) standard for the calibration curve. Then, pooled samples were prepared according to the Filter Aided Sample Preparation (FASP) method. 50 µg of proteins was digested for each pool by using trypsin (Promega, Madison, WI, USA). For protein label-free identification and quantification, tryptic peptides from each sample were analyzed in triplicate by LC-MS/MS using a Proxeon EASY-nLCII (Thermo Fisher Scientific, Milan, Italy) chromatographic system coupled to a Maxis HD UHR-TOF (Bruker Daltonics GmbH, Bremen, Germany) mass spectrometer as already described (Pieragostino *et al*, 2019).

Proteomics data processing

Proteomics raw data were processed using a free computational platform, MaxQuant version 1.6.6.0 (Max-Planck Institute for Biochemistry, Martinsried, Germany). Peak lists, generated in MaxQuant, were searched using Andromeda peptide search engine against the UniProt database (released 2019_11, taxonomy *Mus Musculus*, 21,990 entries) supplemented with frequently observed contaminants and containing forward and reverse sequences. Carbamidomethylation of cysteines (C) was defined as fixed modification, while oxidation of methionines (M) and deamidation of asparagines (N) and glutamines (Q) were set as variable modifications. Mass tolerances were set by default to 0.07 Da in the first search and 0.006 Da in the main search, instead TOF MS/MS match tolerance was set to 0.05 Da. A retention time tolerance of 0.7 min was used to align any time shift in acquisition between samples. For quantitative analysis, we considered proteins identified with a minimum of one peptide. The false discovery rate (FDR) at the protein level was set at 2%, on the contrary, at the peptide level was set at 1% (Madonna *et al*, 2020). Intensity-based absolute quantification (iBAQ) was used to quantify protein abundance in each sample. Bioinformatics analysis was performed with Perseus version 1.6.2.3. In order to define the proteins differentially expressed between samples, a univariate statistical analysis was performed with a *P*-value threshold of 0.05. Protein ratio between sample groups was used as protein expression input for functional analysis using Ingenuity Pathway Analysis (IPA tool, Ingenuity Systems, Mountain View, CA) as previously described (Potenza *et al*, 2021). Briefly, IPA is able to predict the activation (z-scores ≥ 2.0) or inhibition (z-scores ≤ -2.0) of transcriptional regulators or downstreams for the loaded dataset based on prior knowledge of expected effects from published literature citations stored in the IPA system. Data are available via ProteomeXchange with identifier pxd033440.

RT–PCR and qRT–PCR

RNA was extracted from homogenized mouse organs or from cells using TRIzol reagent (Euromedex) following the standard protocol. RNA was translated to cDNA with SuperscriptIII reverse transcriptase (Invitrogen) using Random Hexamers (Invitrogen). Quantitative RT–PCR was applied under standard conditions using SYBR Green (Roche) on a LightCycler 480 (Roche). The relative mRNA expression levels of each gene were expressed as the N-fold difference in target gene expression relative to the *Tbp* gene. Following primers were used: TGAGACTGGGGATGTCTGTAGCTC (Il-6 forward), GGC AACTGGATGGAAGTCTCTTGC (Il-6 reverse); AGCAGTTCAGTAGC TATGAGCCAGA (Tbp forward), GGGAAGGCAGGAGAACATGGC (Tbp reverse).

Sample processing for RNA sequencing (RNA-seq)

CFs were isolated from the distal colons of 6-week-old mice, cultured for two passages, and treated for 24 h in presence of the control and inflammatory conditioned medium, as described above. Total RNA was extracted from each sample using the Maxwell® RSC Instrument (Promega, Madison, WI, USA) and Maxwell RSC simplyRNA Blood Kit (AS1380, Promega). High-quality total RNA was obtained (RNA Integrity Number > 7). RNA-seq libraries were prepared using the NEBNext rRNA Depletion Kit (NEB #E6310, New England Biolabs, Ipswich, MA, USA) and NEBNext Ultra II Directional RNA Library Prep Kit (NEB #E776) for Illumina, following the manufacturer's instructions. The total RNA input was 300 ng per library preparation. The quality and quantity of each library were assessed by the Agilent 2200 TapeStation System (Agilent HS D1000 Assay Kit; Agilent, Santa Clara, CA, USA) and the Qubit Fluorometer (Qubit dsDNA BR Assay Kit; Thermo Fisher Scientific, Waltham, MA, USA), respectively. Each indexed library was reduced to 4 nM before being pooled in equimolar amounts. Library mix was then loaded at a concentration of 1.6 pM and sequenced on a NextSeq500 sequencer from Illumina (San Diego, CA, USA) with a configuration of 150 cycles paired-end reads.

Bioinformatics analyses

Quantification of the transcript reads was performed using the Kallisto program (Bray *et al*, 2016), with default settings and the transcriptome from the NCBI mm10/GRCm38 genome as reference. Raw data are available in the NCBI's Gene Expression Omnibus (GEO) database (GEO; https://www.ncbi.nlm.nih.gov/geo/query/acc.cgi?acc=GSE207877).

The next steps were performed in the R environment 3.5.1. Genes with at least three nonzero samples and a mean of three reads by non-null sample were kept for the downstream analysis steps. To perform the data normalization and the differential expression analysis (DEA) of CM-DSS-CF versus CM-CTL-CF paired samples, we ran standard steps of DESeq2 on the filtered data. We applied a cutoff threshold of 0.01 to the adjusted *P*-values and a cutoff threshold of 2 to the absolute fold changes, resulting in a list of 782 significantly differentially expressed genes (479 upregulated and 303 downregulated in DSS). To study functions involved in the inflamed colon fibroblasts we searched for enrichment with the 50-hallmark gene sets from the MSigDB v7.5.1 Molecular Signatures Database (https://www.gsea-msigdb.org/gsea/msigdb) by computing their metagene score. For a given sample the metagene score is defined by the mean expression of the gene set. The corresponding mouse orthologs of the human genes have been used. We compared the metagene scores of inf-CM and co-CM-treated fibroblast samples using a two-sided *t*-test. Differentially expressed metagenes were defined as significant by a P-value < 0.05.

Statistical analysis

All statistical analysis was performed employing GraphPad Prism version 5. More precisely, we first validated the normal distribution of values (using KS normality test, D'Agostino–Pearson omnibus normality test, Shapiro–Wilk normality test). Then, the values of the different groups were analyzed by the unpaired *t*-test if the variances of the groups were not significantly different and the unpaired *t*-test with a Welch's correction if the variances were significantly different. If values were not normally distributed, a nonparametric Mann–Whitney test was used.

Data availability

The datasets produced in this study are available in the following databases. Microarray data at Gene Expression Omnibus:

https://www.ncbi.nlm.nih.gov/geo/query/acc.cgi?acc=GSE207877. Secretome data at ProteomeXchange (identifier pxd033440): https://www.ebi.ac.uk/pride/archive/projects/PXD033440/.

Expanded View for this article is available online.

Acknowledgments

We are grateful to the excellent platforms in Montpellier, i.e., Montpellier Ressources Imagerie platform, the histology and animal experimentation platforms RHEM and RAM, as well as the IGMM mouse facility ZEFI. Many thanks to Thierry Gostan and the platform SERANAD for help with the statistical analysis. This work was supported by INCA (project 2014-215, to MH, CJ), Plan Cancer et Cancer Inserm-ITMO Aviesan 2021 (to MH, CJ, EM), ANR (AAPG2021, CILCOL to MH, CJ, EM), and by the SFNGE (Grant FARE) to MS and TE. The authors are thankful to Professor Kollias BSRC Fleming Greece, for providing the Col6-Cre mice, Professors Goldstein and Yoder for making available *Kif3aflx/flx* and *IFT88flx/flx* strains, respectively, and to Dr. Stephanie Gofflot, Biobank CHU Liege for providing clinical information. Computing resources for the RNA-seq primary analysis were provided by the computing facilities DISC (Datacenter IT and Scientific Computing) of the Centre de Recherche en Cancérologie de Marseille.

Author contributions

Conception Paul: Conceptualization; formal analysis; investigation; methodology. **Ruizhi Tang:** Formal analysis; investigation; methodology. **Ciro Longobardi:** Conceptualization; formal analysis; investigation; methodology. **Rossano Lattanzio:** Conceptualization; formal analysis; investigation; methodology. **Thibaut Eguether:** Investigation; methodology. **Hulya Turali:** Formal analysis; investigation; methodology. **Julie Bremond:** Formal analysis; investigation; methodology. **Chloe Maurizy:** Formal analysis; investigation; methodology. **Monica Gabola:** Formal analysis; investigation; methodology. **Sophie Poupeau:** Formal analysis; investigation; methodology. **Andrei Turtoi:** Investigation; methodology. **Emilie Denicolai:** Investigation; methodology. **Maria Concetta Cufaro:** Investigation; methodology. **Magali Svrcek:** Resources; investigation. **Philippe Seksik:** Resources. **Vincent Castronovo:** Resources; investigation. **Philippe Delvenne:** Resources; investigation. **Vincenzo De Laurenzi:** Conceptualization; investigation. **Quentin Da-Costa:** Formal analysis; investigation; methodology. **François Bertucci:** Resources; investigation. **Bénédicte Lemmers:** Formal analysis; investigation; methodology. **Damiana Pieragostino:** Formal analysis; investigation; methodology. **Émilie Mamessier:** Conceptualization; formal analysis; investigation; methodology; writing—original draft; writing—review and editing. **Carsten Janke:** Conceptualization; formal analysis; investigation; writing—original draft; writing—review and editing. **Valerie Pinet:** Conceptualization; formal analysis; investigation; methodology; writing—original draft; writing—review and editing. **Michael Hahne:** Conceptualization; supervision; funding acquisition; validation; writing—original draft; writing—review and editing.

Disclosure and competing interests statement

The authors declare that they have no conflict of interest.

References

Armaka M, Apostolaki M, Jacques P, Kontoyiannis DL, Elewaut D, Kollias G (2008) Mesenchymal cell targeting by TNF as a common pathogenic principle in chronic inflammatory joint and intestinal diseases. *J Exp Med* 205: 331 – 337

Bray NL, Pimentel H, Melsted P, Pachter L (2016) Near-optimal probabilistic RNA-seq quantification. *Nat Biotechnol* 34: 525 – 527

Caspary T, Larkins CE, Anderson KV (2007) The graded response to Sonic Hedgehog depends on cilia architecture. *Dev Cell* 12: 767 – 778

Chassaing B, Aitken JD, Malleshappa M, Vijay-Kumar M (2014) Dextran sulfate sodium (DSS)-induced colitis in mice. *Curr Protoc Immunol* 104: 15.25.1 – 15.25.14

Choi JY, Bae J-E, Kim JB, Jo DS, Park NY, Kim YH, Lee HJ, Kim SH, Kim SH, Jeon HB *et al* (2021) 2-IPMA ameliorates PM2.5-induced inflammation by promoting primary ciliogenesis in RPE cells. *Molecules* 26: 5409

Coy S, Du Z, Sheu S-H, Woo T, Rodriguez FJ, Kieran MW, Santagata S (2016) Distinct patterns of primary and motile cilia in Rathke's cleft cysts and craniopharyngioma subtypes. *Mod Pathol* 29: 1446 – 1459

Delaval B, Bright A, Lawson ND, Doxsey S (2011) The cilia protein IFT88 is required for spindle orientation in mitosis. *Nat Cell Biol* 13: 461 – 468

Dinsmore C, Reiter JF (2016) Endothelial primary cilia inhibit atherosclerosis. *EMBO Rep* 17: 156 – 166

Dvorak J, Hadzi Nikolov D, Dusek L, Filipova A, Richter I, Buka D, Ryska A, Mokry J, Filip S, Melichar B *et al* (2016) Prognostic significance of the frequency of primary cilia in cells of small bowel and colorectal adenocarcinoma. *J BUON* 21: 1233 – 1241

Eguether T, Hahne M (2018) Mixed signals from the cell's antennae: primary cilia in cancer. *EMBO Rep* 19: e46589

Eichele DD, Kharbanda KK (2017) Dextran sodium sulfate colitis murine model: an indispensable tool for advancing our understanding of inflammatory bowel diseases pathogenesis. *World J Gastroenterol* 23: 6016 – 6029

Fessler E, Drost J, van Hooff SR, Linnekamp JF, Wang X, Jansen M, De Sousa E, Melo F, Prasetyanti PR, IJspeert JE *et al* (2016) TGFβ signaling directs serrated adenomas to the mesenchymal colorectal cancer subtype. *EMBO Mol Med* 8: 745 – 760

Gadadhar S, Dadi H, Bodakuntla S, Schnitzler A, Bièche I, Rusconi F, Janke C (2017) Tubulin glycylation controls primary cilia length. *J Cell Biol* 216: 2701 – 2713

Gerdes JM, Davis EE, Katsanis N (2009) The vertebrate primary cilium in development, homeostasis, and disease. *Cell* 137: 32 – 45

Gerling M, Büller NVJA, Kirn LM, Joost S, Frings O, Englert B, Bergström Å, Kuiper RV, Blaas L, Wielenga MCB *et al* (2016) Stromal Hedgehog signalling is downregulated in colon cancer and its restoration restrains tumour growth. *Nat Commun* 7: 12321

Gradilone SA, Radtke BN, Bogert PS, Huang BQ, Gajdos GB, LaRusso NF (2013) HDAC6 inhibition restores ciliary expression and decreases tumor growth. *Cancer Res* 73: 2259 – 2270

Guinney J, Dienstmann R, Wang X, de Reyniès A, Schlicker A, Soneson C, Marisa L, Roepman P, Nyamundanda G, Angelino P *et al* (2015) The consensus molecular subtypes of colorectal cancer. *Nat Med* 21: 1350 – 1356

Han Y-G, Kim HJ, Dlugosz AA, Ellison DW, Gilbertson RJ, Alvarez-Buylla A (2009) Dual and opposing roles of primary cilia in medulloblastoma development. *Nat Med* 15: 1062 – 1065

Hao XP, Lucero CM, Turkbey B, Bernardo ML, Morcock DR, Deleage C, Trubey CM, Smedley J, Klatt NR, Giavedoni LD *et al* (2015) Experimental colitis in SIV-uninfected rhesus macaques recapitulates important features of pathogenic SIV infection. *Nat Commun* 6: 8020

Haycraft CJ, Zhang Q, Song B, Jackson WS, Detloff PJ, Serra R, Yoder BK (2007) Intraflagellar transport is essential for endochondral bone formation. *Dev Camb Engl* 134: 307 – 316

Johansson MEV, Gustafsson JK, Sjöberg KE, Petersson J, Holm L, Sjövall H, Hansson GC (2010) Bacteria penetrate the inner mucus layer before inflammation in the dextran sulfate colitis model. *PLoS One* 5: e12238

Karin M, Clevers H (2016) Reparative inflammation takes charge of tissue regeneration. *Nature* 529: 307 – 315

Ko JY, Park JH (2013) Mouse models of polycystic kidney disease induced by defects of ciliary proteins. *BMB Rep* 46: 73 – 79

Kodani A, Salomé Sirerol-Piquer M, Seol A, Garcia-Verdugo JM, Reiter JF (2013) Kif3a interacts with Dynactin subunit p150 Glued to organize centriole subdistal appendages. *EMBO J* 32: 597 – 607

Koliaraki V, Pasparakis M, Kollias G (2015) IKKβ in intestinal mesenchymal cells promotes initiation of colitis-associated cancer. *J Exp Med* 212: 2235 – 2251

Koliaraki V, Prados A, Armaka M, Kollias G (2020) The mesenchymal context in inflammation, immunity and cancer. *Nat Immunol* 21: 974 – 982

Kuhn KA, Manieri NA, Liu T-C, Stappenbeck TS (2014) IL-6 stimulates intestinal epithelial proliferation and repair after injury. *PLoS One* 9: e114195

Kurahashi M, Nakano Y, Peri LE, Townsend JB, Ward SM, Sanders KM (2013) A novel population of subepithelial platelet-derived growth factor receptor α-positive cells in the mouse and human colon. *Am J Physiol Gastrointest Liver Physiol* 304: G823 – G834

Lee SM, Kim N, Son HJ, Park JH, Nam RH, Ham MH, Choi D, Sohn SH, Shin E, Hwang Y-J *et al* (2016) The effect of sex on the azoxymethane/dextran sulfate sodium-treated mice model of colon cancer. *J Cancer Prev* 21: 271 – 278

Liu H, Kiseleva AA, Golemis EA (2018) Ciliary signalling in cancer. *Nat Rev Cancer* 18: 511 – 524

Madonna R, Pieragostino D, Cufaro MC, Doria V, Del Boccio P, Deidda M, Pierdomenico SD, Dessalvi CC, De Caterina R, Mercuro G (2020) Ponatinib induces vascular toxicity through the Notch-1 signaling pathway. *J Clin Med* 9: E820

Malvezzi M, Carioli G, Bertuccio P, Boffetta P, Levi F, La Vecchia C, Negri E (2018) European cancer mortality predictions for the year 2018 with focus on colorectal cancer. *Ann Oncol* 29: 1016 – 1022

el Marjou F, Janssen K-P, Chang BH-J, Li M, Hindie V, Chan L, Louvard D, Chambon P, Metzger D, Robine S (2004) Tissue-specific and inducible Cre-mediated recombination in the gut epithelium. *Genesis* 39: 186 – 193

Marszalek JR, Ruiz-Lozano P, Roberts E, Chien KR, Goldstein LS (1999) Situs inversus and embryonic ciliary morphogenesis defects in mouse mutants lacking the KIF3A subunit of kinesin-II. *Proc Natl Acad Sci USA* 96: 5043 – 5048

Medema JP, Vermeulen L (2011) Microenvironmental regulation of stem cells in intestinal homeostasis and cancer. *Nature* 474: 318 – 326

Minoo P, Zlobec I, Peterson M, Terracciano L, Lugli A (2010) Characterization of rectal, proximal and distal colon cancers based on clinicopathological, molecular and protein profiles. *Int J Oncol* 37: 707 – 718

Naito Y, Takagi T, Uchiyama K, Kuroda M, Kokura S, Ichikawa H, Yanagisawa R, Inoue K-I, Takano H, Satoh M *et al* (2004) Reduced intestinal inflammation induced by dextran sodium sulfate in interleukin-6-deficient mice. *Int J Mol Med* 14: 191 – 196

Onfroy-Roy L, Hamel D, Malaquin L, Ferrand A (2021) Colon fibroblasts and inflammation: sparring partners in colorectal cancer initiation? *Cancers* 13: 1749

Pieragostino D, Lanuti P, Cicalini I, Cufaro MC, Ciccocioppo F, Ronci M, Simeone P, Onofrj M, van der Pol E, Fontana A *et al* (2019) Proteomics characterization of extracellular vesicles sorted by flow cytometry reveals a disease-specific molecular cross-talk from cerebrospinal fluid and tears in multiple sclerosis. *J Proteomics* 204: 103403

Potenza F, Cufaro MC, Di Biase L, Panella V, Di Campli A, Ruggieri AG, Dufrusine B, Restelli E, Pietrangelo L, Protasi F *et al* (2021) Proteomic analysis of Marinesco-Sjogren syndrome fibroblasts indicates pro-survival metabolic adaptation to SIL1 loss. *Int J Mol Sci* 22: 12449

Rocha C, Papon L, Cacheux W, Marques Sousa P, Lascano V, Tort O, Giordano T, Vacher S, Lemmers B, Mariani P *et al* (2014) Tubulin glycylases are required for primary cilia, control of cell proliferation and tumor development in colon. *EMBO J* 33: 2247 – 2260

Roulis M, Flavell RA (2016) Fibroblasts and myofibroblasts of the intestinal lamina propria in physiology and disease. *Differentiation* 92: 116 – 131

Roulis M, Nikolaou C, Kotsaki E, Kaffe E, Karagianni N, Koliaraki V, Salpea K, Ragoussis J, Aidinis V, Martini E *et al* (2014) Intestinal myofibroblast-specific Tpl2-Cox-2-PGE2 pathway links innate sensing to epithelial homeostasis. *Proc Natl Acad Sci USA* 111: E4658 – E4667

Schumacher N, Rose-John S (2019) ADAM17 Activity and IL-6 Trans-Signaling in Inflammation and Cancer. *Cancers (Basel)* 11: 1736

Song CJ, Zimmerman KA, Henke SJ, Yoder BK (2017) Inflammation and fibrosis in polycystic kidney disease. *Results Probl Cell Differ* 60: 323 – 344

Suzuki R, Kohno H, Sugie S, Tanaka T (2004) Sequential observations on the occurrence of preneoplastic and neoplastic lesions in mouse colon treated with azoxymethane and dextran sodium sulfate. *Cancer Sci* 95: 721 – 727

Tanaka T (2012) Development of an inflammation-associated colorectal cancer model and its application for research on carcinogenesis and chemoprevention. *Int J Inflamm*: 2012 , 658786

Taniguchi K, Moroishi T, de Jong PR, Krawczyk M, Grebbin BM, Luo H, Xu R-H, Golob-Schwarzl N, Schweiger C, Wang K *et al* (2017) YAP-IL-6ST autoregulatory loop activated on APC loss controls colonic tumorigenesis. *Proc Natl Acad Sci USA* 114: 1643 – 1648

Todoric J, Antonucci L, Karin M (2016) Targeting inflammation in cancer prevention and therapy. *Cancer Prev Res (Phila)* 9: 895 – 905

Waldner MJ, Foersch S, Neurath MF (2012) Interleukin-6--a key regulator of colorectal cancer development. *Int J Biol Sci* 8: 1248 – 1253

Washington MK, Powell AE, Sullivan R, Sundberg JP, Wright N, Coffey RJ, Dove WF (2013) Pathology of rodent models of intestinal cancer: progress report and recommendations. *Gastroenterology* 144: 705 – 717

Westbrook AM, Wei B, Braun J, Schiestl RH (2009) Intestinal mucosal inflammation leads to systemic genotoxicity in mice. *Cancer Res* 69: 4827 – 4834

Wirtz S, Neufert C, Weigmann B, Neurath MF (2007) Chemically induced mouse models of intestinal inflammation. *Nat Protoc* 2: 541 – 546

Wloga D, Joachimiak E, Louka P, Gaertig J (2017) Posttranslational modifications of tubulin and cilia. *Cold Spring Harb Perspect Biol* 9: a028159

Wong SY, Seol AD, So P-L, Ermilov AN, Bichakjian CK, Epstein EH, Dlugosz AA, Reiter JF (2009) Primary cilia can both mediate and suppress Hedgehog pathway-dependent tumorigenesis. *Nat Med* 15: 1055 – 1061

Expanded View Figures

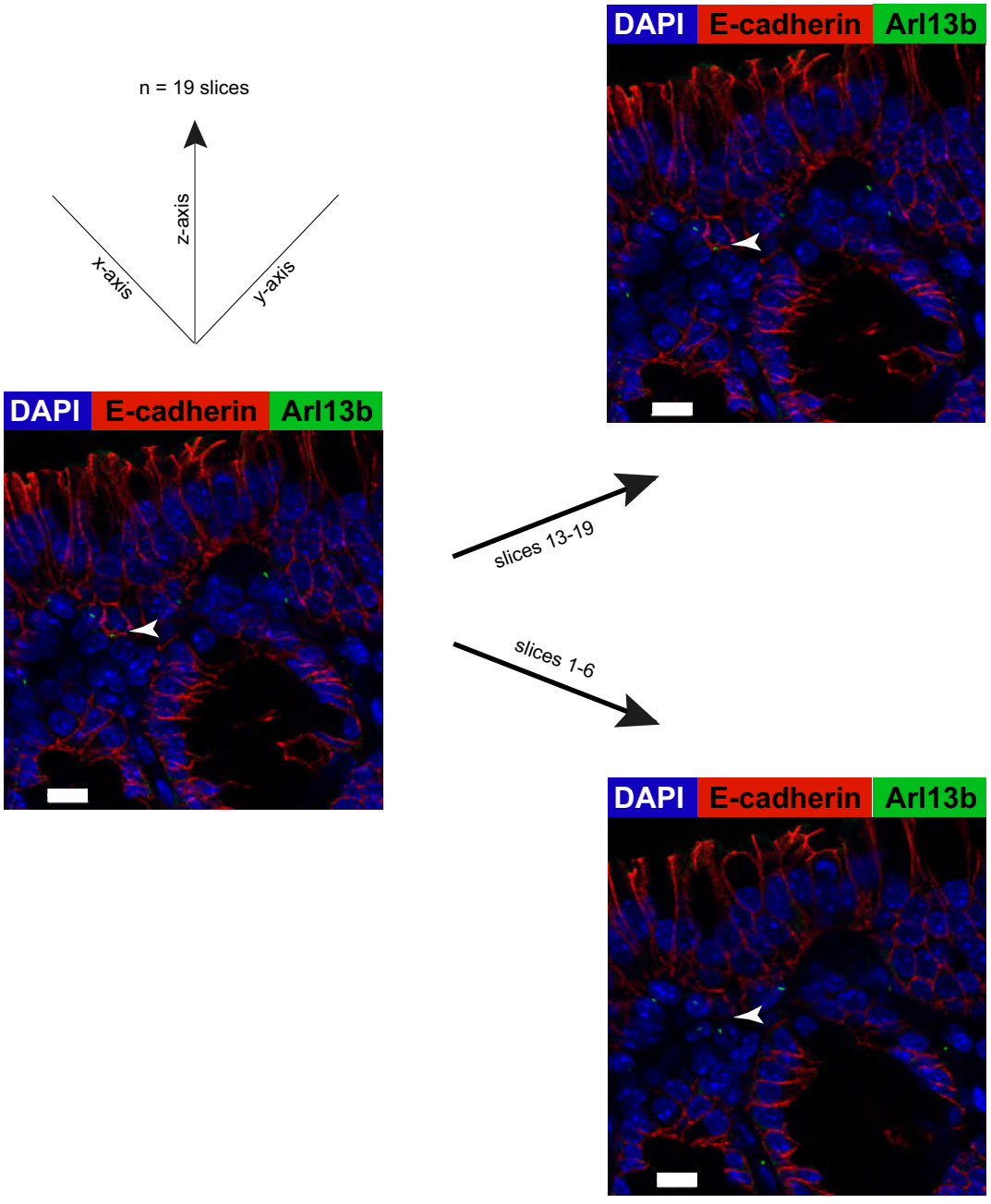

Figure EV1. Primary cilia are expressed by few E-cadherin$^+$ colonic epithelial cells.

Co-staining was performed for E-cadherin (red) and for primary cilia with Arl13b (arrowhead). Different z-stack slices are shown to validate the co-expression of Arl13b and E-cadherin (slices 13–19 represent 1.2 μm thickness). Nuclei were stained with DAPI (in blue). Scale bar represents 10 μm.

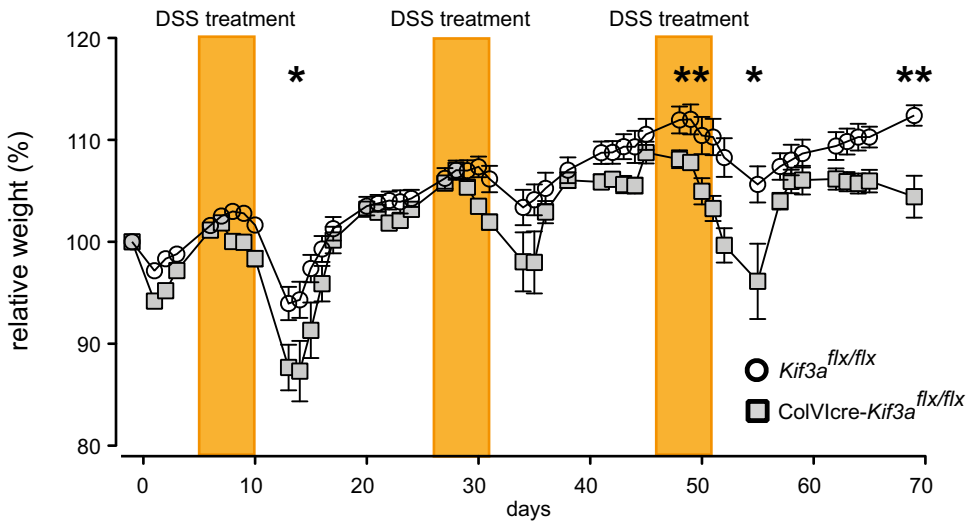

Figure EV2. *ColVIcre-Kif3a*$^{flx/flx}$ mice are more susceptible to DSS treatment during the CAC protocol.

Relative weight of control ($n = 7$) and *ColVIcre-Kif3a*$^{flx/flx}$ ($n = 7$) female mice exposed to the AOM/DSS protocol as described in Fig 4E. Error bars represent standard deviation. *$p < 0.05$, **$p < 0.01$ by two-tailed unpaired *t*-test at indicated time points.

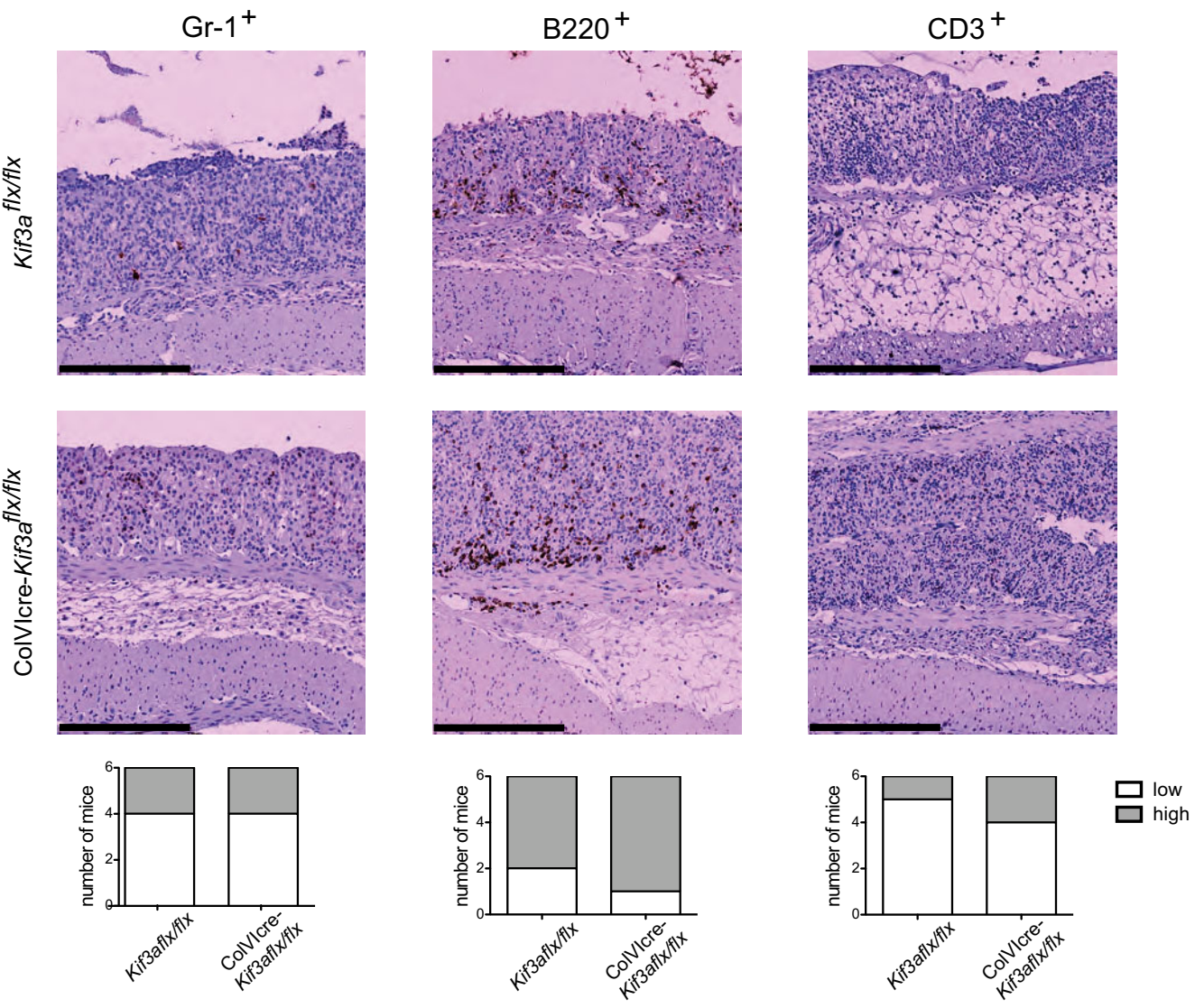

Figure EV3. Numbers of Gr1$^+$ granulocytes, B220$^+$ B cells, and CD3$^+$ T cells are similar in colons of DSS-treated *ColVIcre-Kif3a$^{flx/flx}$* mice.

Mice were treated with DSS as described in Fig 4A. Representative images are shown. At least five fields in the regions of crypt loss were analyzed from each colon of control (n = 6) and *ColVIcre-Kif3a$^{flx/flx}$* (n = 6) mice. Mean cell numbers were scored as low (< 500 cells/mm^2) or high (> 500 cells/mm^2). Scale bar represents 250 μm.

Figure EV4. Low passage primary colonic fibroblast (CF) cultures plus starvation mimic the *in vivo* proportion of PC on CF in an intact colon.

CF were isolated from control and *ColVIcre-Ift88$^{flx/flx}$* mice as described in the Materials and Methods section, passed twice (2P-CF) at days 5–7 and 9–11, and exposed to starvation at day 15 after isolation for indicated time points.

A Representative images of primary CF isolated from *Ift88$^{flx/flx}$* and *ColVIcre-Ift88$^{flx/flx}$* mice starved 24 h (right panels) or not (left panels) to induce primary cilia expression. Primary cilia were stained with Arl13b (in green) and nuclei with DAPI (in blue). Scale bars represent 20 μm.

B Kinetics of PC presence at different time points upon induction of starvation. CF cultures were isolated from distinct animals (n = 3 for each time point). Error bars represent standard deviation. *$p < 0.05$, **$p < 0.01$, ****$p < 10^{-4}$ by two-tailed unpaired t-test.

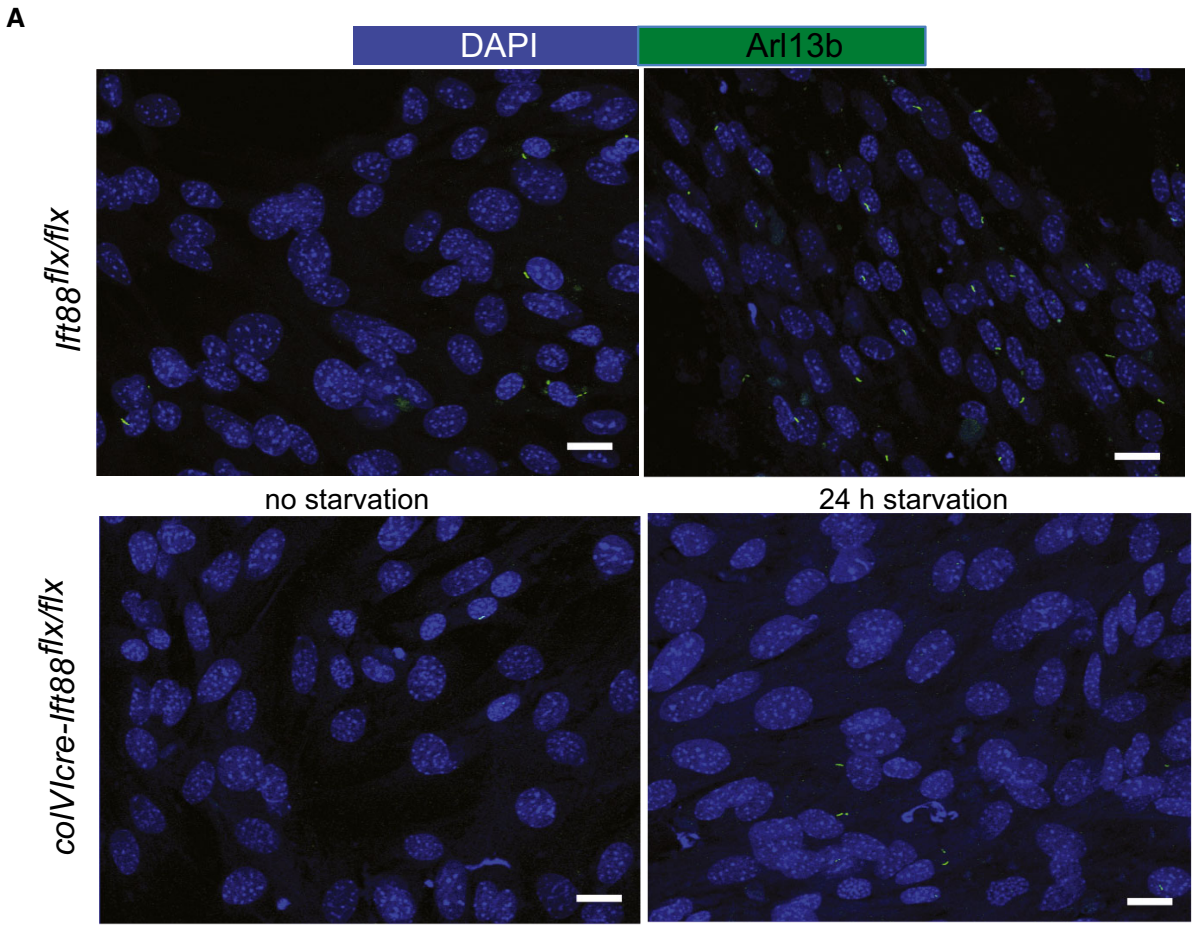

Figure EV4.

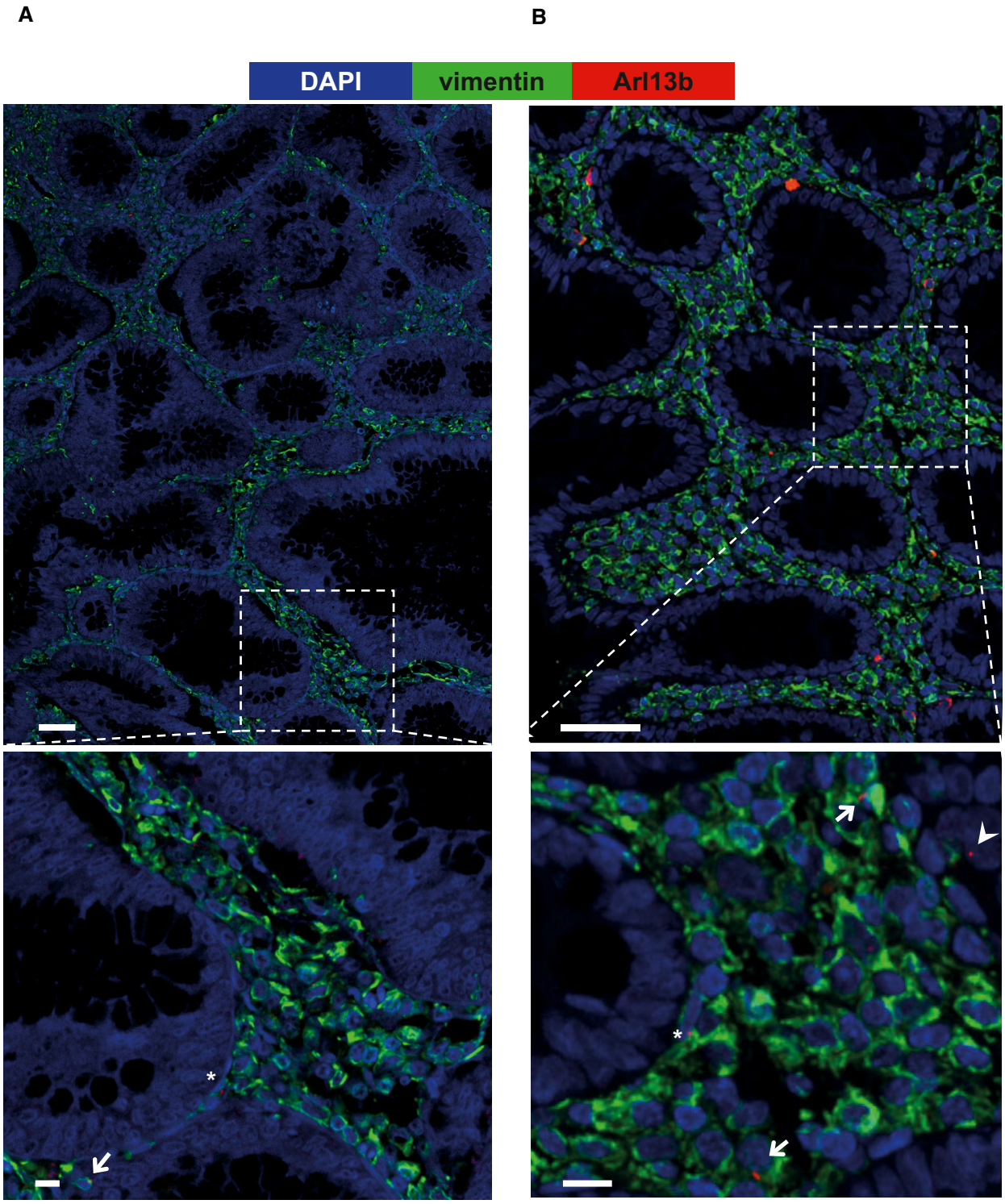

Figure EV5. Stage I CRC tumors display the decreased number of PC.

A, B Representative images of the tissue of a stage I CRC patient showing the decreased number of primary cilia in tumoral (A) versus peritumoral (B) tissues. PC are indicated by arrows in vimentin^{positive} fibroblasts and stars in vimentin^{low} endothelial cells with elongated nucleus. Arrowheads indicate vimentin^{negative} epithelial cells. Scale bars represent 50 and 10 μm in the upper and lower panel, respectively.